

Review

A Comparative Review of Metal Oxide Surface Coatings on Three Families of Cathode Materials for Lithium Ion Batteries

Thabang Ronny Somo^{1,*}, Tumiso Eminence Mabokela^{1,*}, Daniel Malesela Teffu¹,
Tshepo Kgokane Sekgobela¹, Brian Ramogayana², Mpitloane Joseph Hato¹
and Kwena Desmond Modibane^{1,*}

¹ Department of Chemistry, School of Physical and Mineral Sciences, University of Limpopo, Private Bag x1106, Sovenga 0727, South Africa; dannyteffu@gmail.com (D.M.T.); tksekgobela@gmail.com (T.K.S.); mpitloane.hato@ul.ac.za (M.J.H.)

² Materials Modelling Centre, School of Physical and Mineral Sciences, University of Limpopo, Private Bag x1106, Sovenga 0727, South Africa; brian.ramogayana@ul.ac.za

* Correspondence: somoronny@gmail.com (T.R.S.); tumisomabokela@gmail.com (T.E.M.); kwena.modibane@ul.ac.za (K.D.M.)

Abstract: In the recent years, lithium-ion batteries have prevailed and dominated as the primary power sources for mobile electronic applications. Equally, their use in electric resources of transportation and other high-level applications is hindered to some certain extent. As a result, innovative fabrication of lithium-ion batteries based on best performing cathode materials should be developed as electrochemical performances of batteries depends largely on the electrode materials. Elemental doping and coating of cathode materials as a way of upgrading Li-ion batteries have gained interest and have modified most of the commonly used cathode materials. This has resulted in enhanced penetration of Li-ions, ionic mobility, electric conductivity and cyclability, with lesser capacity fading compared to traditional parent materials. The current paper reviews the role and effect of metal oxides as coatings for improvement of cathode materials in Li-ion batteries. For layered cathode materials, a clear evaluation of how metal oxide coatings sweep of metal ion dissolution, phase transitions and hydrofluoric acid attacks is detailed. Whereas the effective ways in which metal oxides suppress metal ion dissolution and capacity fading related to spinel cathode materials are explained. Lastly, challenges faced by olivine-type cathode materials, namely; low electronic conductivity and diffusion coefficient of Li⁺ ion, are discussed and recent findings on how metal oxide coatings could curb such limitations are outlined.

Keywords: lithium-ion batteries; electrochemical performance; metal dissolution; metal oxide coating



Citation: Somo, T.R.; Mabokela, T.E.; Teffu, D.M.; Sekgobela, T.K.; Ramogayana, B.; Hato, M.J.; Modibane, K.D. A Comparative Review of Metal Oxide Surface Coatings on Three Families of Cathode Materials for Lithium Ion Batteries. *Coatings* **2021**, *11*, 744. <https://doi.org/10.3390/coatings11070744>

Academic Editor: Yifan Dong

Received: 19 May 2021

Accepted: 15 June 2021

Published: 22 June 2021

Publisher's Note: MDPI stays neutral with regard to jurisdictional claims in published maps and institutional affiliations.



Copyright: © 2021 by the authors. Licensee MDPI, Basel, Switzerland. This article is an open access article distributed under the terms and conditions of the Creative Commons Attribution (CC BY) license (<https://creativecommons.org/licenses/by/4.0/>).

1. Introduction

Lithium ion batteries are known to have arguably an exceptional mixture of high energy and power density, making the science of batteries an outstanding technology within the energy sector, when compared to its counterparts [1]. The success of electric automobiles could address the global concern of greenhouse gas emissions [2], as the dependence of fossil fuels for transportation would be less [3,4]. The high energy efficiency of Li-ion batteries may also allow their use in various electric grid applications, including improving the quality of energy harvested from wind, solar, geothermal and other renewable sources, thus contributing to their more widespread use. As a result, Li-ion batteries are of paramount importance to energy industry, hence research in this field has been interesting ever since their emergence [5]. The emergence of Li-ion batteries constituted of carbon, a non-aqueous electrolyte, and lithium cobaltate (LiCoO₂) came in 1992, with high hopes as being the first rechargeable battery in the near future [6]. Even to this day, Li-ion battery technology is still relevant as it is a vital component in facilitating green transportation systems such as electric vehicles. The increase in the demand of highly

functionalized applications always includes higher power density, higher energy density, excellent charge-discharge cycling performance and more safety. A significant element that prohibits the performance of batteries to its full potential is the active element of the positive electrode. This has resulted in an intensive research, with special attention on oxides compounds based on transition-metal (TM) element, focusing on materials with structural properties that could easily facilitate large mobility of the Li^+ ions in order to transfer energy during the redox reaction. Layered LiCoO_2 materials were then developed [7], while LiMn_2O_4 spinels [8]; Reference [9] and the LiMPO_4 ($M = \text{Fe}, \text{Mn}, \text{etc.}$) olivine caught attention afterwards [10].

Promptly, all these three families have been extensively studied and efficiently utilized to the development of commercial Li-ion batteries. In almost all cases, layered materials are preferred in high-energy batteries [11,12], whereas spinels and olivines are desired in high-power batteries due to their low cost and long-life requirements, respectively [13,14]. Nevertheless, the lithium-insertion materials should satisfy several aspects including chemical stability, capacity, rate capability, toxicity, cost and safety. All of them, however, achieve theoretical specific capacity $> 140 \text{ mAh/g}$ at a potential $> 3.4 \text{ V vs. Li}^0/\text{Li}^+$. Table 1 gives a summary on the electrochemical properties of each family and their structural distinctions are presented in Figure 1. Their classification is based on dimensionality of Li^+ -ions penetration together with the activation energy that is responsible for Li-ion passage in electrode materials [6]. Archetypes are the two-dimensional $\text{Li}[M]\text{O}_2$ with $M = \text{Co}, \text{Ni}, (\text{Ni}_x\text{Co}_{1-x})$ or $(\text{Ni}_x\text{Mn}_y\text{Co}_z)$, the three-dimensional $\text{Li}[X]_2\text{O}_4$ with $X = \text{Mn}, (\text{Mn}_{1-y/2}\text{Li}_{y/2})$ or $(\text{Mn}_{3/4}\text{Ni}_{1/4})$ and unidimensional $\text{Li}[M']\text{PO}_4$ with $M' = \text{Fe}, \text{Mn}, \text{Ni}, \text{Co}$ or $(\text{Fe}_y\text{Mn}_{1-y})$ [15].

Table 1. Electrochemical properties of three families of insertion compounds [6].

Framework	Compound	Specific Capacity ^a (mAh/g)	Average Potential (V vs. Li^0/Li^+)
Layered	LiCoO_2	272 (140)	4.2
	$\text{LiN}_{1/3}\text{Mn}_{1/3}\text{Co}_{1/3}\text{O}_2$	272 (200)	4.0
Spinel	LiMn_2O_4	148 (120)	4.1
	$\text{LiMn}_{3/2}\text{Ni}_{1/2}\text{O}_4$	148 (120)	4.7
Olivine	LiFePO_4	170 (160)	3.45
	$\text{LiFe}_{1/2}\text{Mn}_{1/2}\text{PO}_4$	170 (160)	3.4/4.1

^a Value in parenthesis indicates the practical specific capacity of electrode.

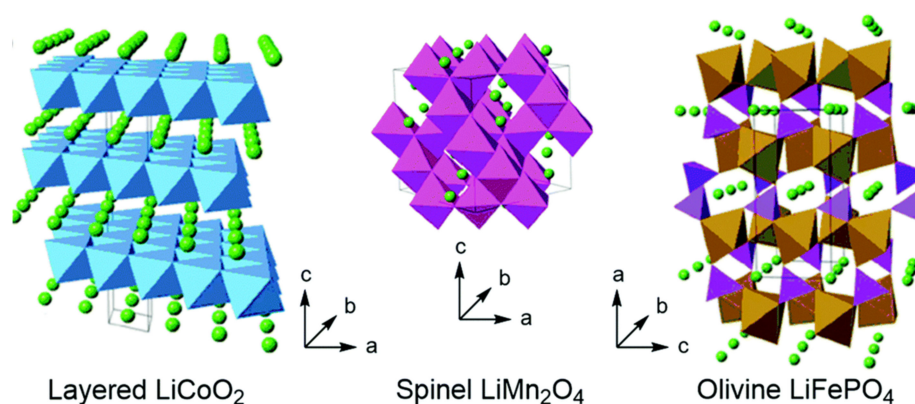


Figure 1. Crystal structures of three families of insertion compounds according to dimensionality of Li^+ -ions diffusion [6].

Regardless of the promising electrochemical properties, which all these three families possess, they share almost similar challenges that can broadly be described as degradation

mechanisms [16,17]. This structural degradation of cathode materials is classified into a number of stages according to the battery functioning procedure: (I) when the cathode material is immersed in the carbonate electrolyte prior to charging, (II) during the primary charging, (III) in the consequent charge/discharge cycles and (IV) during calendar aging [17]. In what follows, degradation mechanism(s) in each stage are discussed succinctly. As a result, the last decade and a half have been populated with many intensive studies, with much discussion focusing on the subsequent impact of these mechanisms for each family of cathode materials [18,19]. Layered cathode materials are more vulnerable to all of these degradation mechanisms, but olivines and spinels are to some extent affected by two or more of the mentioned mechanisms. In any case, results of degradation are very severe as it results in the formation of hydrofluoric acid (HF), side reactions between cathode material and the electrolyte, microcracks in cathode particles, phase transitions and loss of lattice oxygen. Shaw and Ashuri [19] reported in their review article that coating is a potent method to enhance electrochemical performance of $\text{Li}(\text{Ni}_x\text{Mn}_y\text{Co}_z)\text{O}_2$ cathodes for Li-ion batteries as it prevents most of these drawbacks. Similarly, Guan et al. [20] reported recent progress surface coating on cathode materials and mentioned that coating can improve electrochemical properties through enhancing the conductivity, providing structural stability of materials, while limiting side reactions between the electrode and electrolyte. The authors reviewed a wide range of coatings, including metal oxides, metals, fluoride and silicates, and the coating mechanisms. An interesting review by Chen et al. [21] discussed and elaborated on different configurations of coatings, namely, rough coating, core shell structure coating and ultra-thin film coating. Rough coating involves mechanical mixing of cathode materials with coating material followed by heat treatment to form a coated cathode surface. With core-shell structure coating, the coating material is continuously deposited onto the surface of the bulk cathode material until a protective shell is formed. On the other hand, ultra-thin film coating have a thickness down to the subnanometer, compared to the core-shell technique with a thickness up to 1 micrometer. In our previous work [22], which reviewed the effect of metal oxide coatings on hydrogen storage properties of several materials, we noted that amongst several catalytic materials available as coating materials, metal oxides prevail simply because they achieve a core-shell synergistic interaction and their economic efficiency.

The present article reviews the recent developments in metal oxide coatings of three different families of cathode materials for Li-ion batteries, with in-depth discussion on the impact of coating on the degradation mechanism. To the best of our knowledge, this is the first time that a review reports the effect of metal oxide coatings on electrochemical and structural properties of cathode materials. Oh et al. [23] touched on this topic, however, their focus was on the assessment of several coating materials and not a comparison of different metal oxides. Furthermore, the authors paid much attention only on layered LiCoO_2 material. The current review is divided into three sessions according to cathode material families (layered, spinel and olivine materials). For each family, degradation mechanisms are detailed and suitable metal oxide candidates that could address such mechanisms while improving their performance are discussed. Cathode materials could benefit from metal oxide coatings through the following: protection from electrolytes, prevention of electrolyte decomposition, stabilization of surface reactions and provide conductive media [5]. Finally, future viewpoints are presented with the purpose of providing further discussion and ideas on the rational design of coatings for long-lasting and better performing cathodes for the advancing Li-ion batteries in the proximate future.

2. Battery Degradation

Just upon their discovery, Li-ion batteries occurred as the battery of choice for a wide range of applications. Regardless of this establishment, the search for materials that possess improved energy density, better cyclability and reliable safety than conventional Li-ion batteries based on intercalation electrodes is still ongoing. A move to improved-capacity electrode materials is hindered by numerous factors. This section provides a

brief summary on how each cathode family is affected structural and electrochemical degradation mechanisms.

Wu [24] investigated layered cathode materials' prone to degradation by using Kelvin probe force microscopy to study the structural deformation of LiCoO_2 within several cycles. It was noted that an irreversible growth in grain size, decreased surface potential, and irreversible capacity fade all occurred within at most 20 cycles. Ex-situ mechanical measurements on LiCoO_2 films reveal that metrics including the fracture toughness, the elastic modulus and the hardness all decrease by 40%–70% in samples subjected to a single charge–discharge cycle [25]. These changes were correlated with microfractures of LiCoO_2 grains, which is speculated to initiate crack formation and propagation in this material. The use of thin, Li^+ permeable coatings, such as metal oxide layers, improves cyclability for several layered cathode materials. The mechanical degradation of olivine cathode materials was extensively studied in Reference [26], and it was found degradation of the PVDF binder used in the cathode is the main cause of drastic decline in modulus of elasticity and hardness, rather than the active material itself. The degradation is greatly affected by the cycling rate with samples cycled to 90% capacity retention showing a 75% vs. 23% decline in the modulus of elasticity and a 60% vs. 19% loss in hardness for samples cycled at 2 C vs. 1 C. The thin films without any binder showed smaller changes in mechanical parameters following cycling, highlighting the importance of optimizing the stability of the binder used in the cathode. Mechanical degradation of the spinel materials is often correlated with capacity fading mechanisms. For example, a SEM image of LiMn_2O_4 After the first cycle revealed particle microfractures [27]. Additionally, X-ray and neutron diffraction studies in the same study also revealed that crystallinity is lost after the first cycle, and further microstructure analyses showed cracks that are well distributed throughout the material's surface, specifically the (111) crystallographic plane, and twisted fringes point toward internal stress, leading to microscale structural collapse [27]. To deal with the issue of degradation of spinel materials, coating materials presenting protective layers have received considerable attention as outlined in the next sections.

3. Layered Cathode Materials

As shown in Table 1, layered cathode materials for Li-ion batteries are lithium cobalt oxide (LiCoO_2) and $\text{Li}(\text{Ni}_x\text{Mn}_y\text{Co}_z)\text{O}_2$ where $x + y + z = 1$. These materials are classified as two-dimensional materials, based on the Li^+ -ion insertion. LiCoO_2 has enjoyed great dominance in the Li-ion cathode material market due to its theoretical capacity of 272 mAh/g, excellent rate capacity and stable electrochemical properties [28,29]. Commercially, LiCoO_2 has been used extensively in portable electronics due to highly accessible lithium diffusion pathway and a capacity of 140 mAh/g at the potential window 3.6–4.2 V [29–31]. Despite its exceptional properties, the material suffers irreversible capacity loss due to transition metal dissolution into the electrolyte and side reaction with electrolyte during charge/discharge cycling. The electrolyte reacts with even the slightest amount of moisture to produce HF, which is known to aggressively corrode electrodes and cause metal dissolution. Production of HF can be avoided by using LiBOB or LiTFSI salts instead of LiPF_6 as lithium salt. Moreover, to illicit higher capacity and performance of the material, the operating voltage window must be extended to over 4.2 V [31]. This presents a challenge because at elevated temperatures and working voltages Co^{3+} ions from the structure are oxidized to Co^{4+} ions, which form thermodynamically unstable structure of the material leading to further deterioration of capacity [29,31]. Another reason for capacity loss is phase change from hexagonal to monoclinic phase during Li deintercalation [32]. Additionally, the cost and accessibility of Co have always been a concern since the emergence of LiCoO_2 [19]. As a result, much efforts have been dedicated in development of a layered cathode material with almost similar performance as LiCoO_2 , but with less costly and higher abundant elements. $\text{Li}(\text{Ni}_x\text{Mn}_y\text{Co}_z)\text{O}_2$ caught much attention to solve the misery of Co, where Co is partially or completely substituted by Mn and Ni transition metals [33,34]. Upon this findings, Boeing Corporation adopted $\text{Li}(\text{Ni}_{1/3}\text{Mn}_{1/3}\text{Co}_{1/3})\text{O}_2$ for commercial use [19]. However,

recent studies indicate that the structural degradation is also common in $\text{Li}(\text{Ni}_x\text{Mn}_y\text{Co}_z)\text{O}_2$, hence, there is a need for surface modification and herein we review modification through metal oxides.

3.1. Hindering Phase Transitions through Metal Oxide Coating

Phase transitions are very common in layered cathode materials, most especially during Li deintercalation [35,36]. When delithiation takes place, metal redox potentials overlap with oxygen 2p energies leading to oxygen anion oxidation and molecular oxygen release. The resulting oxygen vacancies could accelerate phase transition because they provide low-energy pathways for metal ions to migrate from metal layer to Li layer, leading to phase transitions from the layered structure to defect spinel and rock salt structures [37].

A study by Cho et al. [32] have shown that the presence of metal oxide layer on the surface of LiCoO_2 formed through coating suppresses phase transition during Li deintercalation (Figure 2). Metal oxide coatings are helpful in suppression of phase change due to their high fracture toughness; with examples being ZrO_2 (8–12 $\text{MPa}\cdot\text{m}^{1/2}$) and Al_2O_3 (2.7–4.2 $\text{MPa}\cdot\text{m}^{1/2}$) [38]. On the other hand, LiCoO_2 possesses mean fracture toughness of $1.7 \pm 0.4 \text{ MPa}\cdot\text{m}^{1/2}$ while its median fracture toughness is $0.9 \pm 0.4 \text{ MPa}\cdot\text{m}^{1/2}$ [32]. As a result, lattice distortion is minimized or delayed in such a way that hexagonal phase is retained. Therefore, it is very important to note that it would be impossible to suppress phase transition using metal oxides with low fracture toughness that is equivalent to that of LiCoO_2 , such as SiO_2 ($0.77 \text{ MPa}\cdot\text{m}^{1/2}$).

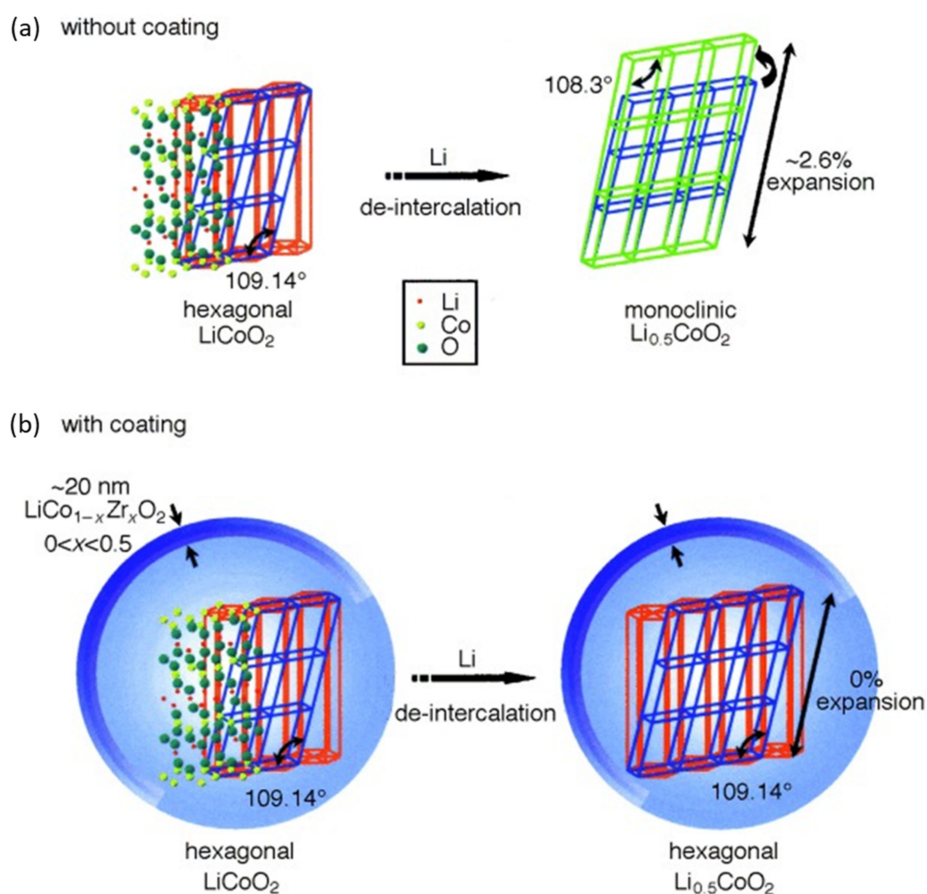


Figure 2. (a) The formation of a monoclinic phase with nonuniform lattice constant expansion (2.6%) in bare LiCoO_2 during charging (Li deintercalation), and (b) the suppression of phase transition from hexagonal to monoclinic phase by a fracture-toughened thin-film metal-oxide coating. Permission from [32] Copyright 2001 John Wiley and Sons.

Another study conducted by Chung et al. [39] explains the mode of phase transition much better. The authors used in situ X-ray diffraction to evaluate phase transformations of uncoated and ZrO₂-coated LiCoO₂ over several charging/discharging cycles in a wider voltage window from 2.5 to 4.8 V. As shown by XRD patterns in Figure 3a, both materials contain Bragg reflections (indexed based on a hexagonal cell) from (0 0 3) to (1 0 4), with the hexagonal (H1) phase being the only present phase [39]. At the end of the charging process to 5.2 V, new phases; namely H2a, H2, O1a and O1 are observed for uncoated sample, with the final phase O1 documented to be forming around 4.8 V, while all initial peaks of H1 phase disappear [39]. On the other hand, the XRD spectra of the coated sample in Figure 3b reveal phase transformation to O1a only. The numbers on the right hand side of the XRD patterns correspond to the charge–discharge cycle number.

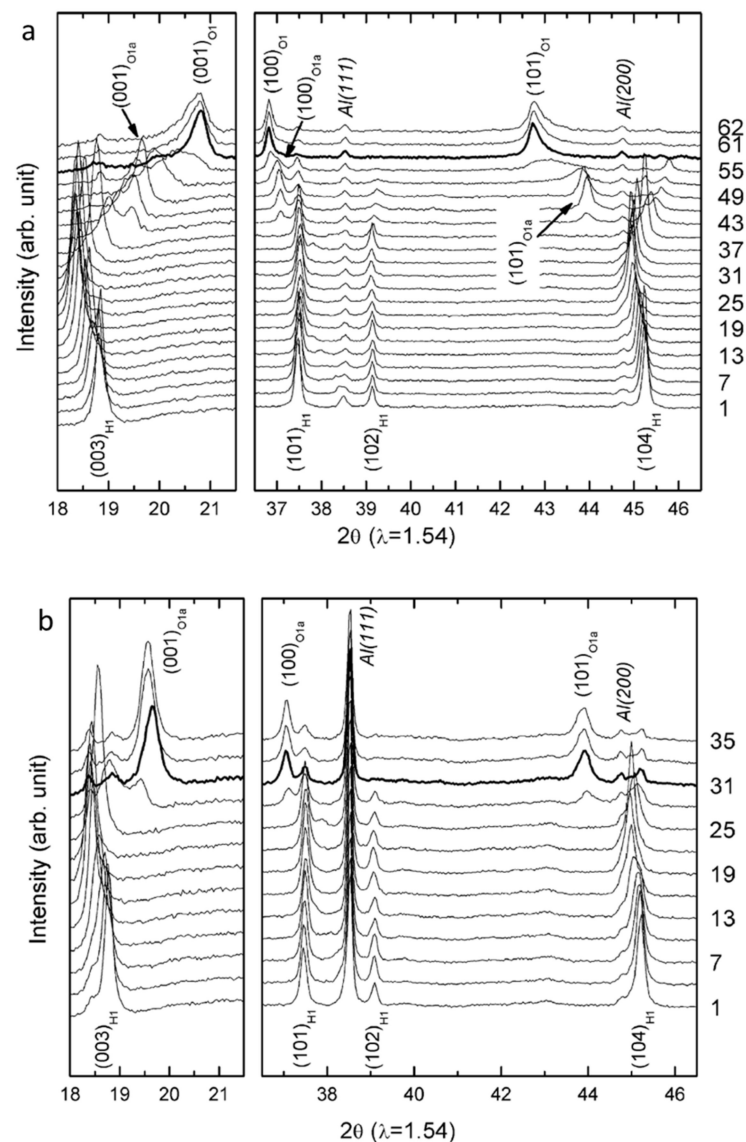


Figure 3. The in situ XRD patterns of (a) uncoated LiCoO₂ and (b) ZrO₂-coated LiCoO₂ collected during charge to 5.2 V in the (0 0 3)–(1 0 4) region. Permission from [39] Copyright 2006 Elsevier.

Among the four peaks of hexagonal phase, the (1 0 2)H1 peak is the only peak that disappeared upon complete charge, signifying that the original phase was maintained even up to 5.2 V [39]. Similar observations were reported for Al₂O₃-Coated LiCoO₂ [40], SnO₂-Coated LiCoO₂ [41], La₂O₃-coated LiCoO₂ [42] and CeO₂-coated LiCoO₂ [43].

3.2. Preventing Metal ion Dissolution

Lithium Mn-Ni-Co oxides have been reported to experience metal ion dissolution during charging/discharging cycles. For materials containing Mn, the metal dissolves when Mn^{3+} ions undergo a disproportionation reaction to form Mn^{2+} and Mn^{4+} . The second metal ion-related challenge that still needs attention for applications of lithium Mn-Ni-Co oxides is the cation mixing between Ni^{2+} (0.69 Å) and Li^+ (0.76 Å) ions, as their ionic radii are almost equivalent [44]. The cation mixing between these two ions on the crystallographic (3b) sites is known to deteriorate their electrochemical performance [6]. A study by Kim et al. [45] revealed that the amount of cobalt dissolution from LiCoO_2 material immersed in an electrolyte for a week at room temperature is 260 ppm as depicted in Figure 4. The parent material was compared with metal oxide (SiO_2 , B_2O_3 , TiO_2 , Al_2O_3 and ZrO_2) coated material. A very negligible amount of cobalt was dissolved for ZrO_2 -coated LiCoO_2 material under similar conditions. This almost zero Co dissolution is related to lattice distortion suppression by metal oxide deposition.

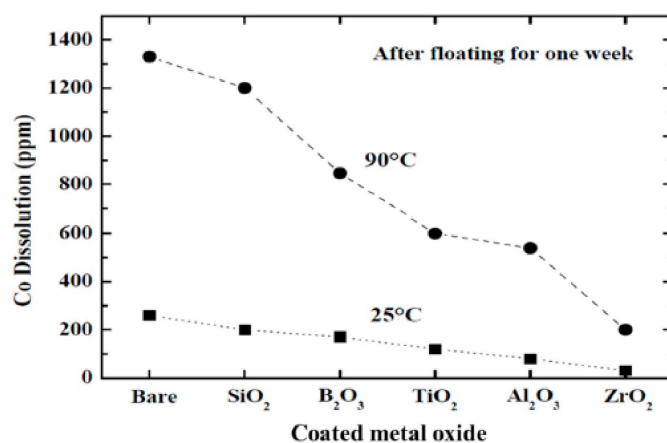


Figure 4. The amount of cobalt dissolution in the electrolyte, from metal-oxide coated and uncoated LiCoO_2 after an initial charge to 4.4 V, and being immersed for one week at 25 °C and 90 °C. Permission from [45] Copyright 2003 IOP.

3.3. Scavenging Hydrofluoric Acid Attacks

HF normally forms when LiPF_6 from the electrolyte breaks down to react with moisture, which is always found in LiPF_6 -containing electrolyte [46]. Subsequently, the generated HF then attacks the cathode material to react with Li_2O , dismantling and dissolving the cathode material into the electrolyte. All these take place according to the following three reactions in Equations (1)–(3) [19].



This means that Li-ion-based cathode materials are vulnerable to such attacks and as a result surface modification through metal oxides could form a protective layer that is strong enough to eliminate such surface reactions. For example, Myung and coworkers [44] reported a very useful study about HF attack on Al_2O_3 -coated $\text{Li}[\text{Li}_{0.05}\text{Ni}_{0.4}\text{Co}_{0.15}\text{Mn}_{0.4}]\text{O}_2$ electrode. The analyses were done using transmission electron microscopy (TEM) and time-of-flight secondary ion mass spectrometry (ToF-SIMS), depicted in Figures 5 and 6, respectively. Figure 5b–d clearly shows the metal oxide layer on the smooth surface of the parent material. For small quantities of coatings, Al_2O_3 particles appeared to be meso-sized while nano-sized particles were observed when the coating quantity was increased to 2.5%. The surface attack on Al_2O_3 -coated $\text{Li}[\text{Li}_{0.05}\text{Ni}_{0.4}\text{Co}_{0.15}\text{Mn}_{0.4}]\text{O}_2$ by HF was qualitatively

discussed by ToF-SIMS, as this instrument can detect molecule ions qualitatively for surface analysis. Since uncoated material is directly exposed to HF, HF easily targets and reacts with Ni, Co and Mn elements of the cathode material to produce byproducts on the surface of the active material over several cycles of charging.

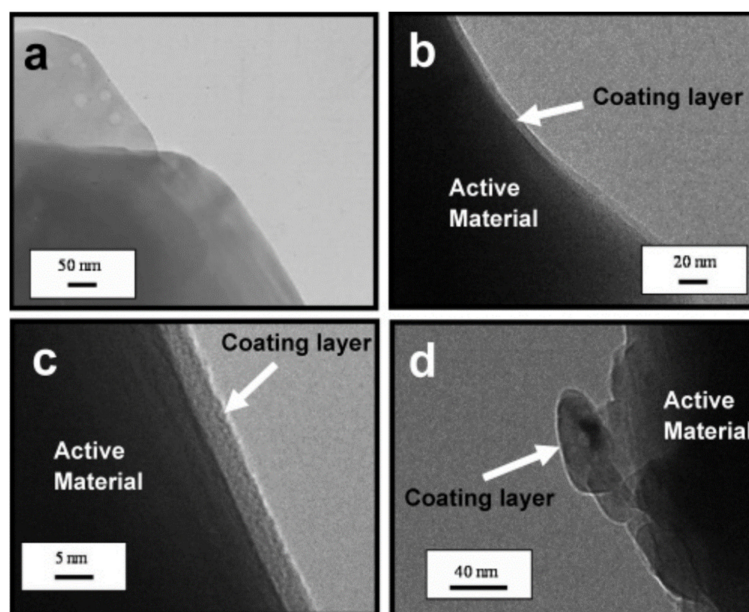


Figure 5. TEM bright-field images of (a) bare and Al_2O_3 -coated $\text{Li}[\text{Li}_{0.05}\text{-Ni}_{0.4}\text{Co}_{0.15}\text{Mn}_{0.4}]\text{O}_2$ (b–d): (b) 0.25 wt.% of Al_2O_3 -coated (at lower magnification), (c) 0.25 wt.% of Al_2O_3 -coated (at higher magnification) and (d) 2.5 wt.% of Al_2O_3 -coated $\text{Li}[\text{Li}_{0.05}\text{Ni}_{0.4}\text{Co}_{0.15}\text{Mn}_{0.4}]\text{O}_2$. Permission from [47] Copyright 2005 American Chemical Society.

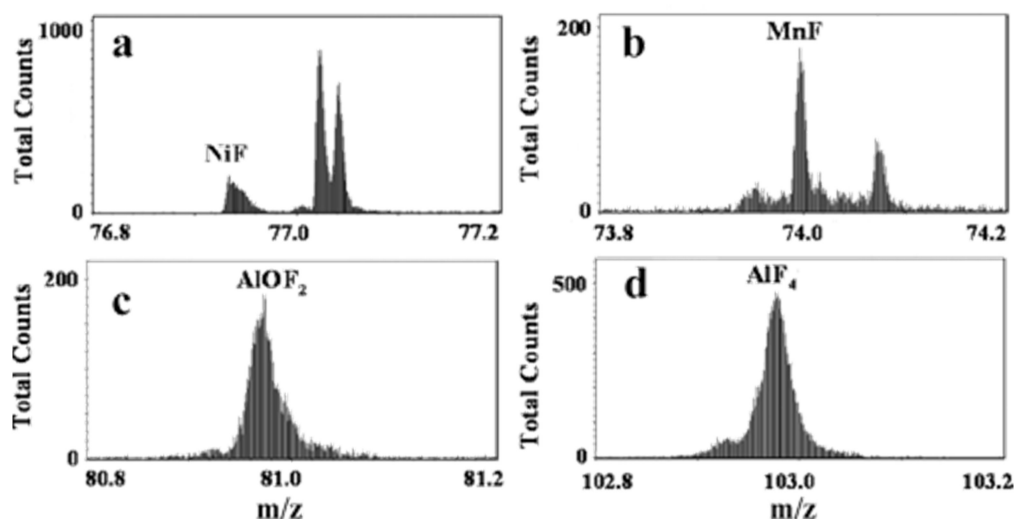
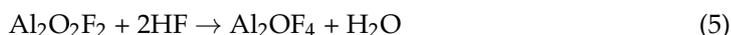


Figure 6. ToF-SIMS results (high mass resolution spectra) of extensively cycled Al_2O_3 -coated $\text{Li}[\text{Li}_{0.05}\text{Ni}_{0.4}\text{Co}_{0.15}\text{Mn}_{0.4}]\text{O}_2$ electrode at $60\text{ }^\circ\text{C}$. Permission from [47] Copyright 2005 American Chemical Society.

Then, the byproducts would be detected as fragments having Ni-F and Mn-F bonding as seen in Figure 6a,b. However, in a case of Al_2O_3 coated material, the coating layer is the only layer directly exposed to HF and therefore initial reaction would be between HF and Al_2O_3 layer to produce Al-O-F and Al-F fragments, as shown revealed by mass

resolution spectra in Figure 6c,d. As a result, the following reactions in Equations (4)–(6) would take place:



This reaction delays or even eliminates the possibility of the acid attack on parent material and consequently improves the performance of the cathode to a full potential.

Aykol et al. [48] analyzed various ranges of *s*-, *p*- and *d*-block binary metal oxides and fluorides as coating materials using a DFT-based thermodynamic design framework to study the HF-scavenging mechanisms as suggested in experiments (Figure 7). Comparing their results with the available experimental data helped demonstrate that the HF-scavenging is more effective only when the fluoride layer can be formed as a product of the reaction.

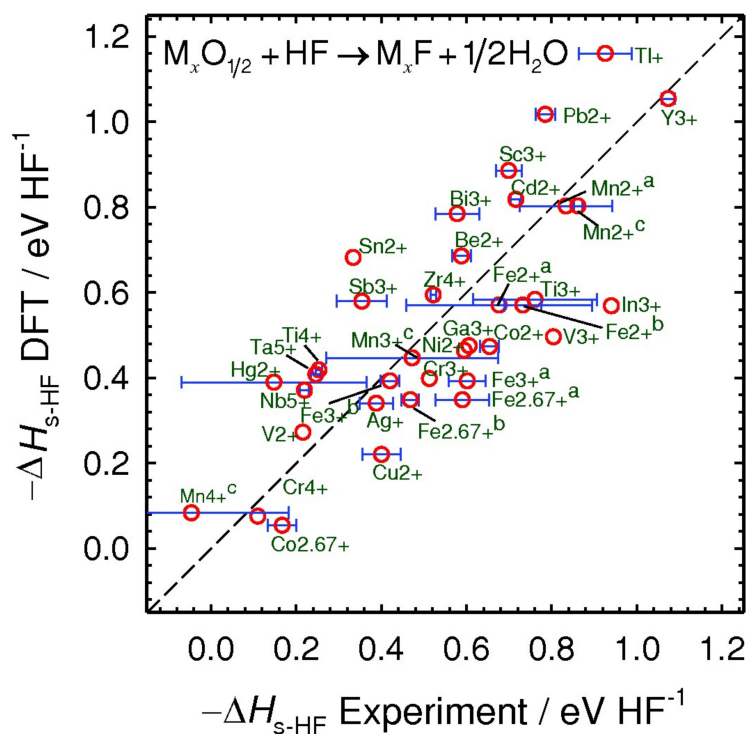


Figure 7. Comparison of HF-scavenging reaction enthalpies of *p*- and *d*-block metal oxides calculated by DFT. The error-bars show combined standard uncertainties (CSUs) in experimental values. Permission from [48] Copyright 2014 John Wiley and Sons.

3.4. Improved Electrochemical Performance

A study by Shim et al. [49] reported on the synthesis of magnesium oxide (MgO) coated LiCoO₂ cathode materials at varied annealing temperatures (750–810 °C). The coated samples showed remarkable capacity retention as high as 85% and improved initial discharge capacity as shown in Table 2. It was found that the best performing MgO@LiCoO₂ material (annealed at 810 °C) exhibited 85% capacity retention after 60 cycles, with the uncoated LiCoO₂ only exhibiting 72.8% after the same number of cycles [49]. Through transmission emission microscopy (TEM) images of the best performing MgO@LiCoO₂ sample, Shim and coworkers [49] were able to establish the existence of some competitive substitutions on the Li sites by Mg ions from the coating. The Mg ions acted as “point defect pillars” and held the Li⁺ diffusion pathways open and clear for smoother ion movement, which lead to enhanced capacity, better cycling performance and preserved the structural integrity. This observed “point defect pillars” type of mechanism is not unique as it was

formally proposed by Sayle et al. [50] in lithium manganese oxide (Li_2MnO_3) cathode materials. Interestingly, improvements in both the rate capability and initial discharge capacity were observed by He et al. [51] in their study of Al-Ti-oxide coated LiCoO_2 as can be shown in Table 1. In their case, some competitive substitutions on the cobalt (Co) site by aluminum (Al) was observed [51]. This behavior is similar to that observed in MgO@LiCoO_2 samples annealed at lower temperatures, were competitive ion substitution favored Mg^{2+} substitution at the Co^{3+} sites. In Al-Ti-oxide coated LiCoO_2 , XRD data revealed that the partial substitution of Co^{3+} with Al^{3+} decreased the lattice parameter a and caused a slight increase of the lattice constant c [51]. On the other hand, XRD data of MgO@LiCoO_2 samples annealed at lower temperatures also showed an increase in the value of lattice parameter c due to Mg^{2+} partial substitution at the Co^{3+} sites [49]. This changes in lattice parameter values of a and c are due to the disparity in ionic radius of $\text{Mg}^{2+}/\text{Al}^{3+}$ and Co^{3+} , which then increase the value of the ratio a/c , which is beneficial to Li^+ diffusion [51]. This positive influence on the Li^+ diffusion led to better rate capability and initial discharge capacity [51]. Furthermore, the cyclic voltammograms showed that Al-Ti-oxide coated LiCoO_2 exhibited narrow and sharp peaks than its uncoated counterpart, which indicate faster Li^+ diffusion kinetics [51]. This was further supported by a lower R_{ct} value with indicates a reduced electrode polarization and improvement in the rate capability [51].

Enhancements in the cycling stabilities and rate capabilities of metal oxide coated LiCoO_2 electrodes at higher working potentials has also been reported. Lee et al. [52] synthesized a series of vanadium oxide (V_2O_5) coated LiCoO_2 electrodes and observed an enhancement to the structural stability at increased operating voltages. Similarly, improvements were observed in a study by Hao et al. [53] when they produced copper oxide (CuO) coated LiCoO_2 electrodes. The best performing CuO coated electrode exhibited a greatly enhanced cycle stability of the material by retaining up to 88.85% of the initial capacity at 1 C after 50 cycles [53]. Moreover, the CuO coated electrode performance was outstanding even at rates as high as 5 C. In both cases of V_2O_5 and CuO coated materials, the improvement is the increase in electrode stability at elevated working potentials (4.5 V) and at high-charge cut-off. The presence of order-disorder transition peaks at 4.1 V and 4.2 V in the cyclic voltammograms of CuO coated LiCoO_2 electrodes indicated that the coating did not prevent phase transitions but rather, reduced the peak separation potential. A reduced peak separation potential translates to improved electrochemical performance as the electrochemical polarization is reduced. On the other hand, the enhancements in V_2O_5 coated materials can be attributed to the coating reducing the surface area of active sites of the electrode, which are in contact with the electrolyte therefore preventing Co^{3+} dissolution and electrode/electrolyte side reaction at elevated working potentials [52].

Table 2. Effect of metal oxide coatings on electrochemical properties of layered materials.

Coating	Coating Thickness	Coating Technology	Initial Discharge Capacity (mAh/g)	Capacity Retained (mAh/g)	Rate Capability (mAh/g)	R_{ct} (Ω)	Measurement Conditions	Reference
ZnO	17 nm	Radio Frequency magnetron sputtering	193–191	140–175.53	75–106 (10 C)		3.0–4.5 V, 0.2 C, RT, 50 Cycles	[54]
$\text{Li}_4\text{Ti}_5\text{O}_{12}$	25 nm	Radio Frequency magnetron sputtering	187.88–188.88	121–170	113 (12 C)	522.6–148.7	3.0–4.5 V, 0.2 C, RT, 60 Cycles	[25]
Al-Ti-Oxide	20 nm	Wet chemical method	177.7–189.1	133.1–172.5	146.2–174.4 (1 C)	626.4–348	3.0–3.7 V, 0.2 C, RT, 100 Cycles	[51]
CuO	2 wt. %	Wet chemical method	162–166	110–158	96.5–120 (5 C)	Improved	3.0–4.5 V, 1 C, RT, 50 Cycles	[53]
MgO		Ball milling	150–153	100–132.5	–	–	3.9–4.0 V, 0.2 C, RT, 50 Cycles	[49]
ZrO ₂	1.5 wt. %	Wet chemical method	143–135	137–140	–	Improved	3.0–4.5 V, 0.1 C, RT, 40 Cycles	[55]
TiO ₂	1.5 nm	Wet chemical method	120–133	58–110	16–98 (60 C)	19.01–16	3.0–4.5 V 1 C, RT, 100 Cycles	[56]

Recent research developments in surface coating of electrode materials have pointed in favor of post-coating electrodes as opposed to loose active powders. Metal oxide coating of assembled LiCoO₂-based positive electrodes consisting of the active material, carbon black, N-methyl pyrrolidone (NMP) and polyvinylidene fluoride (PDVP) binder on a current collector have been found to be more effective and delivers enhanced electrode performance [29]. Coating the preassembled electrode as opposed to the bare active material greatly reduces internal resistance of the electrode and allows coating even with electrically insulative coating such as ZnO [29,54]. This is because the coating is formed on the outer most surface of the electrode and thus the electron transport pathways between particles of active material, carbon black and the surface of the current collector are preserved. References [28,29] assembled a positive electrode comprising of LiCoO₂, acetylene black, NMP and PDVP binder using Al foil as the current collector. The electrode was coated with Li₄Ti₁₅O₁₂ via magnetron sputtering and was found to deliver better performance than its uncoated counterpart [29]. The best performing Li₄Ti₁₅O₁₂ coated sample delivered an initial discharge capacity of (188.88 mAh/g) with 90% of this capacity retained (170 mAh/g) even after 60 cycles when compared to only 64.4% retention (121 mAh/g) of the uncoated electrode [29]. From the electrochemical impedance spectroscopy (EIS) measurements performed, a lowering of the charge transfer resistance (R_{ct}) was observed. A reduction in the R_{ct} value is a clear indication of the clearing or shortening of Li⁺ diffusion pathways, which leads to smoother movement of ions and thus improvements in capacity and charge transfer rate. Furthermore, the cycling stability greatly benefited from the corrosion protecting effects of the Li₄Ti₁₅O₁₂ coating, which prevented electrode/electrolyte side reaction responsible for the gradual loss in capacity during cycling.

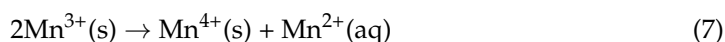
On the other hand, Dai et al. [54] observed similar improvement in LiCoO₂ positive electrode coated with ZnO by the atomic layer deposition method. In their study, it was observed that the coated electrode exhibited a higher capacity retention and rate capacity as observed in Table 2. From cyclic voltammetry (CV) curves, it was established that the voltammetric peak corresponding with Co³⁺ to Co⁴⁺ oxidation, which lead to phase transformation at 4.1 V was absent in the coated electrode [54]. The observed peak suppression indicates that the ZnO coating prevented phase transformation, which induces an irreversible capacity loss [54]. ZnO is known to be a good HF scavenger and can therefore react with HF in the electrolyte to form more stable metal fluorides complexes and prevent formation of solid electrolyte interface (SEI) layer and electrode/electrolyte side reactions [57]. When contrasted with active material coated electrodes, metal oxide coating of assembled LiCoO₂-based positive electrodes exhibit even greater performance as can be seen in Table 2.

4. Spinel Cathode Materials

LiMn₂O₄ spinel type materials have been developed as potential cathode materials in lithium ion batteries for portable electronics and electric vehicle applications [58,59]. This is due to their 3-dimensional Li⁺ diffusion pathways, low toxicity, low cost and abundance of manganese [59,60]. LiMn₂O₄ has a theoretical capacity of 148 mAh.g⁻¹ and practical capacity of 140 mAh.g⁻¹ at operating potential of <4 V vs. Li/Li⁺ [61]. However, this material suffers from capacity fading as a result of Jahn-Teller distortion of Mn³⁺, Mn dissolution into the electrolyte and electrolyte decomposition at >4 V vs. Li/Li⁺ [58,60,61]. Xia et al. [61] in their report suggested that this capacity fading could also be observed even within the 4 V potential window especially at elevated temperatures. Jahn-Teller distortion can be avoided by simply substituting 25% of Mn with Ni in LiMn₂O₄ material to form LiNi_{0.5}Mn_{1.5}O₄ because this composition implies that Mn is in the 4+ valence, thus avoiding the Jahn-Teller distortion associated to Mn³⁺. Therefore, the electrochemical activity is only due to the oxidation/reduction of Ni²⁺ ions leading transfer of 2e⁻ per Ni ion.

4.1. Suppression of Mn Dissolution

It is known that the key problem that hinders the implementation of LiMn_2O_4 and related spinel cathodes is the severe dissolution of Mn in acidic electrolytes, especially at high operational temperatures [62,63]. Upon dissolving, Mn ions migrate out of the cathode to anode material and thus lead to self-discharge of lithiated graphite anode [64,65]. Choi et al. [66] proposed a reasonable mechanism for the dissolution of manganese out of a delithiated LiMn_2O_4 cathode. This mechanism, which involves transition in oxidation state between Mn ions, is depicted in Figure 8. When the cathode is fully delithiated, tetravalent manganese ions (Mn^{4+}) are formed, as shown in Figure 8. Reduction of Mn^{4+} to Mn^{3+} can occur through the acceptance of electrons produced by the oxidative decomposition of the LiPF_6 -based electrolyte. The resulting Mn^{3+} ions undergo a disproportionation reaction, according to the following:



Which takes place on the surface of the cathode material to form Mn^{2+} ions. The dissolved Mn^{2+} ions are the main agents of capacity decrease since a deposit of just one Mn^{2+} ion facilitate extraction of two Li^+ ions out of the lithiated graphite into the cell [67]. Therefore, to obtain high performing Li-ion batteries that are constituted of a spinel cathode material containing Mn, the dissolution of Mn should be minimized. This can be achieved through surface modification and coating using metal oxides, same way as described with layered cathode materials.

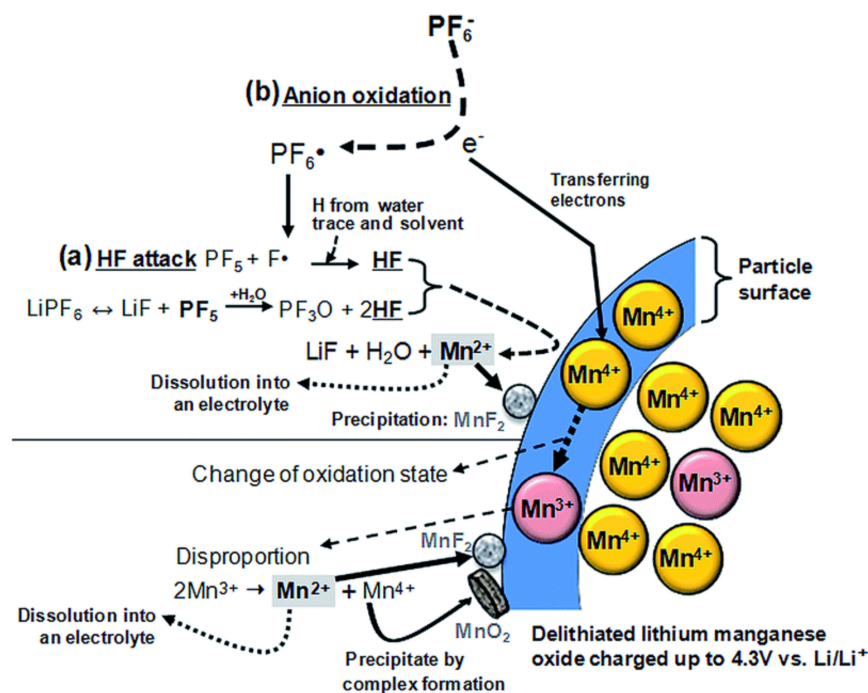


Figure 8. Schematic presentation for the manganese dissolution out of a delithiated LMO cathode (a) by the HF attack and (b) by the PF_6^- anion oxidation. Permission from [66] Copyright 2015 RSC.

An example of such work is summarized in Figure 9, which was conducted by Zhang et al. [58]. In this particular study, LiMn_2O_4 cathode material was coated with Ti_2O to get rid of Mn dissolution, thus improving its electrochemical performance at high temperatures. The material with a 3 wt.% of Ti_2O coating performed better than 1 wt.% and 5 wt.% coatings. The TEM images in Figure 9a reveal an interesting feature as uniform coating of Ti_2O on the surface of parent material changes the (111) plane of spinel LiMn_2O_4 to the (311) plane of the cubic lattice of LiMn_2O_4 . The coating is composed of porous networks connecting directly with the three-dimensional channel of spinel LiMn_2O_4 and can be used

to store Li^+ . Therefore, this structure can easily facilitate Li^+ diffusion with favorable flow kinetics. Their XRD patterns revealed no additional Ti_2O phases upon coating, indicating a favorable non-detectable coating, with no incorporation between the parent material and coating (Figure 9b). After 250 cycles at 55°C , the uncoated material experienced a severe 25.9 wt.% Mn dissolution while only 7.47 wt.% of Mn was dissolved into the electrolyte for 5 wt.%- Ti_2O coated material. This shows the ability of Ti_2O to strongly suppress HF attack on the vulnerable Mn ions.

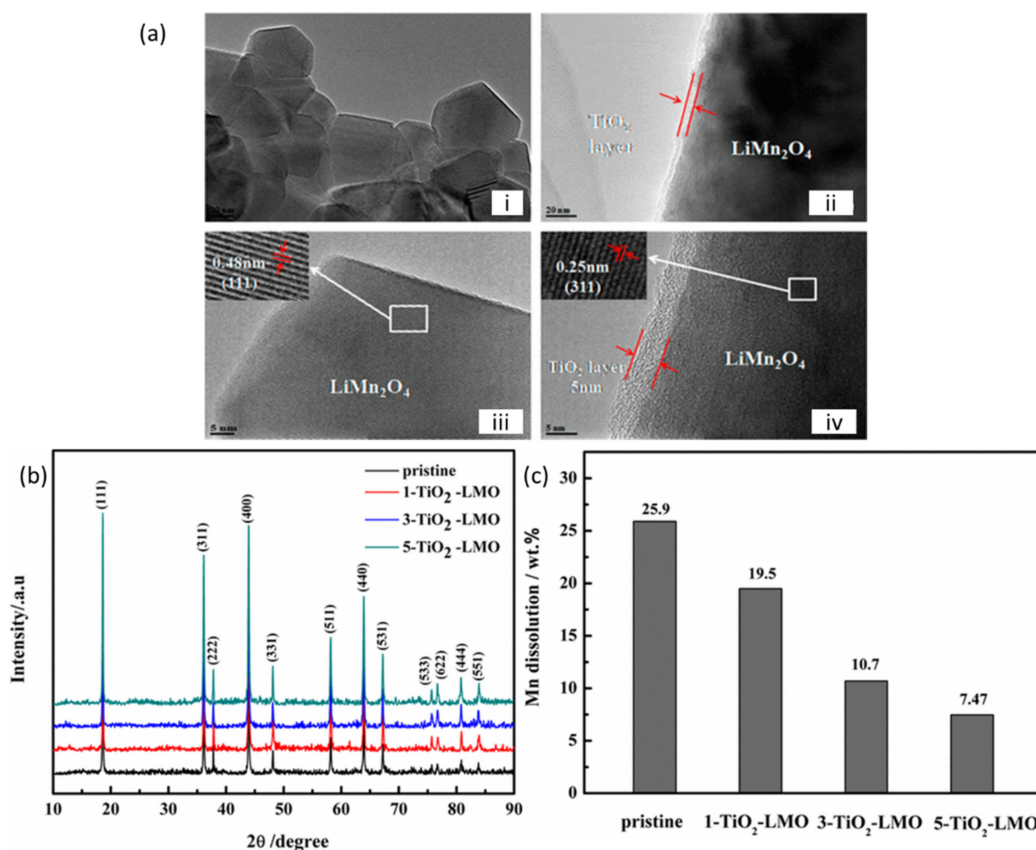


Figure 9. (a) TEM images of (I) uncoated LiMn_2O_4 and (II) $3\text{-TiO}_2\text{-LiMn}_2\text{O}_4$ and HRTEM images of (III) uncoated LiMn_2O_4 and (iv) $3\text{-TiO}_2\text{-LiMn}_2\text{O}_4$. (b) XRD patterns of the pristine and TiO_2 -coated LiMn_2O_4 particles. (c) Weight percent of Mn dissolution of pristine and TiO_2 -coated electrodes after 250 cycles at 55°C . Permission from [58] Copyright 2017 American Chemical Society.

Waller and coworkers [59] also investigated the protective effects of metal oxides on the LiMn_2O_4 electrode. In their work, atomic layer deposition technique was used to apply an aluminum (III) oxide (Al_2O_3) coating on LiMn_2O_4 and study its electrochemical behavior (Figure 10). The best performing Al_2O_3 coated electrode retained superior performance compared to its uncoated counterpart even after 500 cycles and when cycled at different current densities. When examining the Mn 2p photoelectron line of cycled coated electrode under energy-dispersive X-ray spectroscopy (XPS), the authors observed that the uncoated electrode had a slightly decreased oxidation state of Mn while the coated remained unchanged [59]. This suggests that the coating suppressed Mn dissolution into the electrolyte [59]. Furthermore, an increase in the binding energy along the Al 2p photoelectron line in cycled coated electrodes was observed, which suggested a change in Al chemical environment [59]. This was due to Al bonding to a more electronegative species, which is likely fluorine to form Al-F species [59]. This is consistent with literature, which suggests that Al_2O_3 can scavenge HF and prevent corrosion of the electrode.

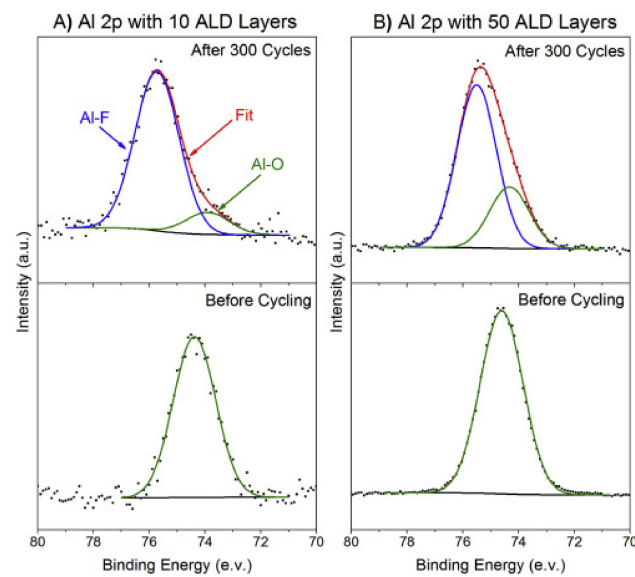


Figure 10. (A) Al 2p spectra of 10-layer Al_2O_3 and (B) 50-layer Al_2O_3 coated LiMn_2O_4 . Permission from [59] Copyright 2016 Elsevier.

Chen et al. [68] discussed a mechanism of Al_2O_3 growth on the spinel LiMn_2O_4 using the in-situ method and computation simulation. In their work, the decomposition of the methyl ($-\text{CH}_3$) group from trimethylaluminum (TMA) to the O atoms on the (111) surface Li/O-terminated was demonstrated (see Figure 11). It was indicated that the early cycles of atomic layer deposition (ALD) led to the reduction of the average Mn oxidation state, with a high ratio of Mn^{3+} because of the high coordination of Al to the surface oxygen. Additionally, indicated some Al doping at the interstitial sites upon ALD, and the sub-monolayer stabilizes defects and result in an improved capacity retention.

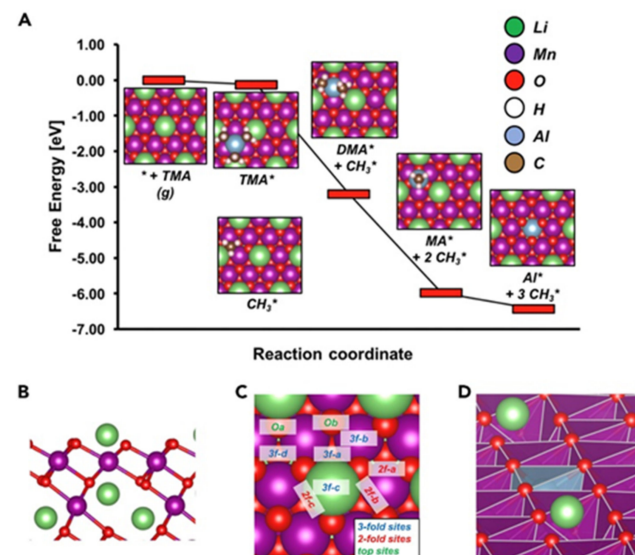


Figure 11. TMA decomposition thermodynamics on Li/O-terminated LMO (111) surface. (A) Free-energy diagram for TMA decomposition through demethylation on the LMO surface. Insets contain corresponding low-energy structural configurations for $\text{Al}(\text{CH}_3)_x^*$ on the surface, along with adsorbed CH_3^* fragments widely separated from one another. (B) Side view of the Li/O-terminated (111) surface. (C) Oxygen top, two-fold, and three-fold adsorption sites on the (111) surface. (D) Alternative angle of low-energy configuration of Al^* species, involving occupation of interstitial 16c sites (3f-c), with octahedral coordination to lattice oxygen atoms. Permission from [68] Copyright 2018 Elsevier.

Warburton et al. [69] later illustrated the comprehensive analysis of acid-based chemistries associated with the ALD reactions using both experimental and theoretical DFT methods as shown in Figure 12. In their study, it was indicated that the TMA loses its $-\text{CH}_3$ resulting in the reduction near-surface Mn^{4+} ion to Mn^{3+} , because of the amphoteric nature of the ligand CH_3 , which favors electron transfer from the adsorbate to the surface, resulting in the reduction near-surface Mn^{4+} ion to Mn^{3+} . Similar mechanism was demonstrated on NMC material for TMA decomposition where methyl binding through O-sites led to near-surface reduction. Considering the undesired Mn^{3+} on the surface, which is susceptible to disproportionation, Ouyang et al. [70] studied the effect of coating with Al_2O_3 on the oxidation states of Mn atom. They indicated that upon coating the LiMn_2O_4 (001) surface with Al_2O_3 , the oxidation state of surface Mn atoms reduced from Mn^{3+} to Mn^{4+} .

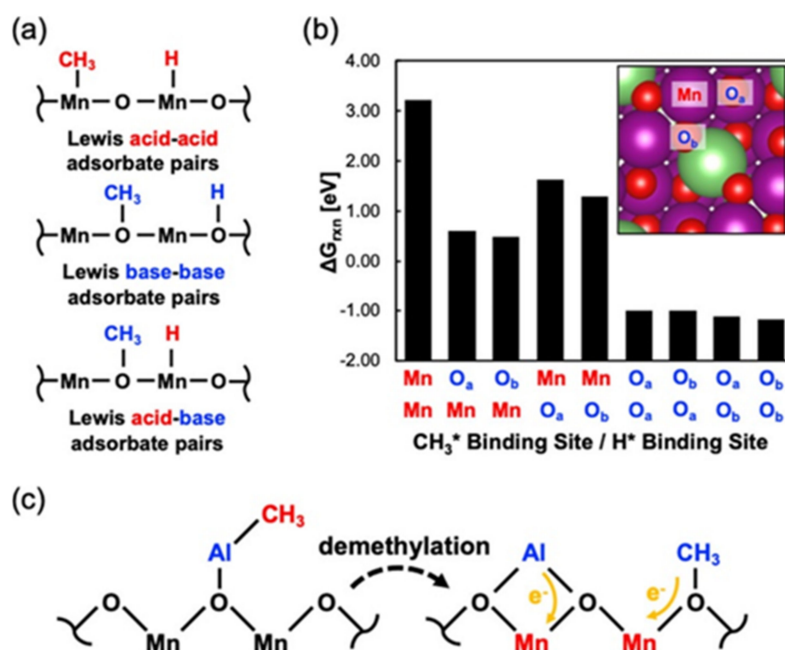


Figure 12. Lewis acid–base chemistry of $-\text{CH}_3$ groups adsorbed on the LMO surface. (a) Configurations of Lewis acid–acid, base–base and acid–base pairs between CH_3^* and H^* adsorbates. The electron donor/acceptor behavior may vary with inclusion of coadsorbates. (b) Adsorption free energies for different CH_3^*/H^* configurations on the Mn/O-terminated LMO (001) surface. Adsorption sites are labeled on the figure in the inset, with Lewis acidic and basic adsorbate configurations indicated by red and blue font, respectively. (c) Schematic of Lewis acid–base chemistry (adsorbate electron accepting and donating behavior) in the context of TMA demethylation on LMO. Upon demethylation, the $-\text{CH}_3$ fragments undergo a change in their donor/acceptor behavior and prefer binding to oxygen atoms on LMO. In this case, two Mn^{4+} ions behave as the Lewis acidic adduct (electron acceptor) to each of the Lewis basic adsorbates. The overall reaction leads LMO to gain two electrons (localized in Mn 3d orbitals) per demethylation event. Permission from [69] Copyright 2020 American Chemical Society.

4.2. Improved Electrochemical Performance

In a study by Feng et al. [71] tungsten(III) oxide (WO_3) was coated onto LiMn_2O_4 cathode material in order to evaluate its protective effects against Mn dissolution into the electrolyte. The best performing coated sample delivered a capacity retention of 89.4% at 1 C when compared to 75.1% from the bare LiMn_2O_4 at room temperature after 50 cycles [71]. Furthermore, the WO_3 coating showed better performance even at higher rates and elevated temperatures as observed in Table 3. Similarly, vanadium (V) pentoxide (V_2O_5) coating on LiMn_2O_4 delivered exception results yielding a 75%–107.3% capacity retention and reversible capacity of $107.3 \text{ mAh}\cdot\text{g}^{-1}$ at 1 C after 200 cycles [72]. On the other hand, Zhang et al. [57] reported on porous TiO_2 coated LiMn_2O_4 , which retained most of

the discharge capacity when compared to the pristine active material. In their study, it was found that the best performing TiO₂ coated LiMn₂O₄ could retain up to 62% capacity at 55 °C while uncoated LiMn₂O₄ retained only 26% of the initial capacity [57].

Table 3. Effect of metal oxide coatings on electrochemical performance of LiMn₂O₄ spinel cathode materials.

Coating	Coating Thickness	Coating Technology	Initial Discharge Capacity (mAh/g)	Capacity Retained (mAh/g)	Rate Capability (mAh/g)	R _{ct} (Ω)	Measurement Conditions	Ref
WO ₃	2 wt. %	Wet chemical method	129.8–126.8	97.48–113.36	78–96 (10 C)	178–57.8	3.3–4.3 V, 1 C, RT, 50 Cycles	[71]
			129.5–125.6	95.31–119.1	–	–	3.3–4.3 V, 1 C, 60 °C	
V ₂ O ₅	2.5 wt. %	Wet chemical method	110.9–125.1	75–107.3	48–108 (2 C)	69.72–26.72	3.0–4.5 V, 1 C, RT	[72]
			76.1–113.5	55–92	38–78 (2 C)	–	3.0–4.5 V, 1 C, 55 °C	
TiO ₂	20–35 nm	Wet chemical method	126.9–126.4	101.9–113.89	–	20–18	3.0–4.5 V, 0.5 C, RT, 250 Cycles	[57]
			126.54–124.35	32.9–77.1	–	–	3.0–4.5 V, 0.5 C, 55 °C, 250 cycles	
MoO ₃	3 wt. %	Wet chemical method	96–101.59	40–70.2	76–28 (10 C)	166.3–81.5	3.5 and 4.3 V, 2 C, RT, 900 Cycles	[60]

5. Olivine Cathode Materials

LiFePO₄ is the representative material for the olivine structure, known for its thermal stability and high-power capability. With theoretical specific capacity 170 mAh/g at moderate current densities, the phospho-olivine LiFePO₄ is less costly and less toxic, as compared to layered and spinel cathode materials for large-scaled applications [73]. However, this material possesses electronic conductivity of approximately 10^{−9} S/cm [74], which is very low. Moreover, low diffusion coefficient of Li⁺ ion (approximately 10^{−14} cm²/s) of LiFePO₄ may result in poor cyclability and subsequently capacity fading [75]. On a positive note, the reduction of the LiFePO₄ particles to the nanosize provides short Li⁺-ion diffusion paths within the positive electrode [76–78]. Additionally, the conductivity of LiFePO₄ is improved through coating of the material with a conductive carbon between particles providing high diffusion kinetics and preventing particles agglomeration [74,77–81].

5.1. Enhancing Electronic Conductivity of Olivine Cathode Materials

Conductivity can be calculated according to Equation (8) below:

$$\sigma = \frac{1/R_{ct}}{t/A} \quad (8)$$

where σ is conductivity, R_{ct} is the charge transfer resistance and t represents the thickness of the electrode while A denotes area of the electrode surface [82]. Although it has been used successfully by many researchers, the above conductivity measurement is affected by difficulty in differentiating between different types of ions and providing rather a reading relative to the combined effect of all ions. Thus, it should be applied with some pre-knowledge of the bulk composition or utilized in moderately pure solutions to be effective. Carbon is favorable for this application due to its cost effectiveness and good effect to control the particle size of LiFePO₄. However, the electrically conductive carbon reduces the tap-density of LiFePO₄, which is being harmful to the energy density of the lithium ion battery [83]. Furthermore, the low-temperature performance of carbon-coated LiFePO₄ also needs to be improved [84]. This is because during the intercalation process, the electrons cannot reach all the positions where Li⁺ ion intercalation takes place, which results in polarization of the electrode [85]. Alternative materials that have the capability to improve electrochemical performance and conductive nature of LiFePO₄ are metal oxides that are first doped with conductive metals such as indium, gallium and aluminum since most metal oxides are insulators [86,87]. Furthermore, metal oxides possess solid density that is much higher than that of LiFePO₄, implying that such combination can enhance electrochemical

performance and tap density of LiFePO_4 . For example, Tang et al. [85] reported that coating of LiFePO_4 by aluminum doped zinc oxide doubled discharge specific capacity of the parent material from 50.3 to 119.4 $\text{mA}\cdot\text{h/g}$. Increased electrical conductivity and tap density upon coating were ascribed as the major driving force for better electrochemical performances. In another study, Liu et al. [86] reported that the ZrO_2 nanocoating increases the mechanical toughness of the core particles and decreases the interface charge transfer resistance, and thus, remarkably enhances the electrochemical performance of the LiFePO_4 cathode. Some authors prefer co-coating of LiFePO_4 with carbon and metal oxides as co-coating facilitates synergic effects on improvement of electrochemical performance [76,88]. An example involving co-coating of LiFePO_4 was reported by Cui et al. [89] through ZnO and carbon. ZnO and carbon co-coated LiFePO_4 cathode possessed a $9.2 \times 10^{-5} \text{ S/cm}$ compared to $4.1 \times 10^{-5} \text{ S/cm}$ of the uncoated cathode, signifying a huge improvement in conductivity.

Jin et al. [90] employed Raman spectroscopy to study the effect of V_2O_3 coating on the conductivity of carbon-coated LiFePO_4 cathode (Figure 13). The authors attributed the two broad peaks that are clearly visible in Figure 11A–C, namely D-band and G-band, to carbon and can be fitted with four separated dotted-line peaks at 1194 (peak 1), 1347 (peak 2), 1510 (peak 3) and 1585 cm^{-1} (peak 4), respectively. Peaks 2 and 4 are contributed by sp^2 -type graphite-like structure (i.e., sp^2 C–C bonds), while peak 1 and peak 3 by sp^3 -type diamond-like structure (i.e., sp^3 C–C bonds), which is often related to amorphous carbon. Hence the integrated intensity ratio $I_{\text{sp}^2}/I_{\text{sp}^3}$ can be used to characterize the degree of graphitization of carbon, where I_{sp^2} and I_{sp^3} are the total areas of (peak 2 + peak 4) and (peak 1 + peak 3), respectively. Figure 13d, which is a plot of $I_{\text{sp}^2}/I_{\text{sp}^3}$ against vanadium content, reveals that the degree of graphitization for the carbon in the LiFePO_4/C composites increases with the content of vanadium. Subsequently, this observation does confirm that V_2O_3 increases the conductivity of the LiFePO_4/C since conductivity of carbon materials is knowingly proportional to degree of graphitization [91].

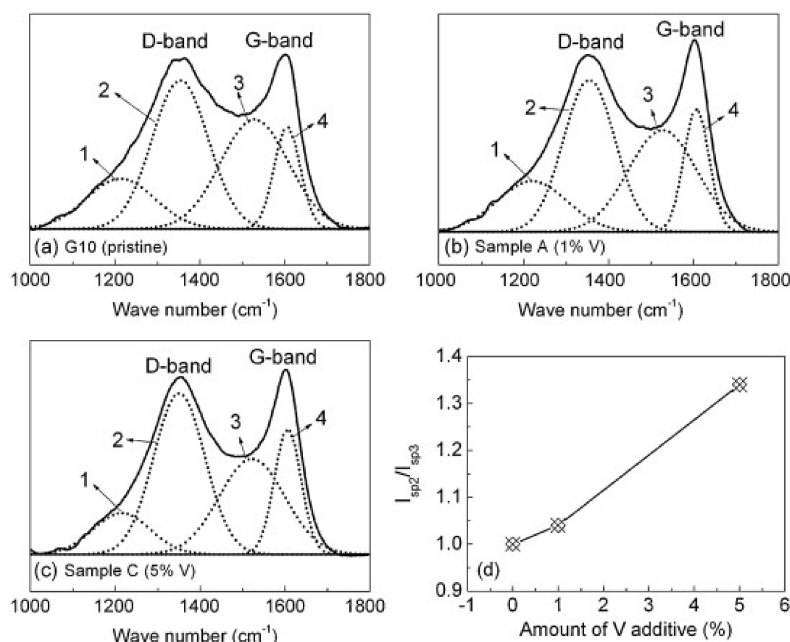


Figure 13. Raman spectra of (a) LiFePO_4/C , (b) 1% V_2O_3 coated LiFePO_4/C and (c) 5% V_2O_3 coated LiFePO_4/C (the dotted lines are from a Gaussian numerical simulation), and (d) the relationship of $I_{\text{sp}^2}/I_{\text{sp}^3}$ vs. V content. Permission from [90] Copyright 2011 Elsevier.

5.2. Improved Electrochemical Performance

Poor energy density, power density, cycle life and safety concerns negatively affect electrochemical performance of olivine-based cathode materials. As previously mentioned,

these materials possess specific capacity of 170 mAh/g, which is very low compared to that of their layered cathode counterparts (272 mAh/g). Coating technology, especially through different metal oxides has received attention in addressing these challenges. Most of metal oxides provide good coatings except AlPO_4 , as it is associated with possible metal dissolution from the bulk material during the coating procedure due to the use of water as a solvent [92]. It has been reported that a thin layer (1 wt.%) of metal oxide on the surface of LiFePO_4 material can enhance the kinetics due to the interparticle resistance and particle size decreasing [93]. The impregnation of ZrO_2 on the LiFePO_4 surface resulted in enhanced electrochemical performance without affecting the structure stability of the parent material [86]. Under 1 C rate, the discharge specific capacity improved from 82 to 97 mAh/g upon coating. The highly conductive TiO_2 material has been reported to improve the cycle performance of the LiFePO_4 cathode at elevated temperatures [87]. The results showed that the coating reduce the capacity fading of $\text{LiFePO}_4/\text{Li}$ cell but imposes an adverse effect on the LiFePO_4/C cell. Table 4 below compares the effect of some metal oxide coatings on olivine cathode materials. All the coated cathode materials presented in the table deliver higher reversible discharge capacity and retain over 90% of the initial capacity after several cycles (check Table 4) as compared to the pristine material. Improvement in electrochemical properties is attributed to the unique core-shell synergistic interaction in the presence of metal oxide layer on the surface of a cathode material.

Table 4. Effect of metal oxide coatings on electrochemical performance of LiFePO_4 olivine cathode materials.

Coating	Coating Thickness	Coating Technology	Initial Discharge Capacity (mAh/g)	Capacity Retained (mAh/g)	Rate Capability (mAh/g)	R_{ct} (Ω)	Measurement Conditions	Reference
ZrO_2	2–3 nm	Chemical Precipitation Method	146	138–143.4	82–94 (1 C)	Improved	1.5–4.5 V, 0.1 C, RT, 100 Cycles	[86]
TiO_2	3 wt.%	Sol gel Method	145	132–140	–	Improved	2.5–4.3 V, 1 C, 55 °C, 90 Cycles	[87]
SiO_2	–	Sol gel Method	150–160	143–155	140–145 (1 C)	Improved	2.5–4.3 V, 0.1 C, RT, 50 Cycles	[94]
CeO_2	2 wt.%	–	153.8	128.7	170 (1 C)	64.3	3.45–3.40 V, 1 C, 20 °C, 30 cycles	[95]
ZnO	–	Chemical Precipitation Method	134.5	147.7	138.5 (0.1 C)	197.5	2.6–4.4, 0.1 C, RT, 100 cycles	[89]

6. Conclusions

The lithium ion-based batteries have clear exceptional advantages when compared to other battery types, including zinc air, silver oxide and nickel metal hydride batteries. Nevertheless, research continues on developing innovative cathode materials to overcome minor and major disadvantages such as cost, energy density, power density, cycle life and safety. Cathode materials that have prevailed over the last decades are the layered two-dimensional $\text{Li}[M]\text{O}_2$ with $M = \text{Co}, \text{Ni}, (\text{Ni}_x\text{Co}_{1-x})$ or $(\text{Ni}_x\text{Mn}_y\text{Co}_z)$, the spinel-type three-dimensional $\text{Li}[X]_2\text{O}_4$ with $X = \text{Mn}, (\text{Mn}_{1-y}/2\text{Li}_y/2)$ or $(\text{Mn}_{3/4}\text{Ni}_{1/4})$ and olivine-type uni-dimensional $\text{Li}[M']\text{PO}_4$ with $M' = \text{Fe}, \text{Mn}, \text{Ni}, \text{Co}$ or $(\text{Fe}_y\text{Mn}_{1-y})$ but each of them have several limitations. Olivine cathode materials suffer from low electrical conductivity and poor lithium ion diffusivity, low thermal stability and high volume expansion. Layered and spinel-type materials are prone to attacks by hydrofluoric acid (HF), side reactions between cathode material and the electrolyte, microcracks in cathode particles, phase transitions and loss of lattice oxygen. Coating methods through metal oxides have been pursued to overcome these challenges. Metal oxide coatings show a great potential as they provide protection from electrolyte, prevention of electrolyte decomposition, stabilization of surface reactions and conductive media. However, the size and uniformity of coating are still major concerns as Li deintercalation in coated cathode materials depends on them and as such, future research should deal much on such factors because achieving a well-controlled coating by metal oxides would be helpful. Increasing and strengthening the cross networking between the metal oxide/parent material layers by increasing surface functional moieties or adding cross-linkers could enhance the proficiency of the cathode materials. Subse-

quently, continuous research and innovative developments are necessary to improve the electrochemical properties of lithium ion batteries. Research associated with the expansion of high technological processing routes for metal-oxides coated nanoarchitected Li-rich layered cathode materials with a precisely controlled composition of Mn, Co, Ni, Al and Mo materials may have a remarkable benefit in the improvement of the battery economy. Many intercalation cathodes have been brought to market, and lithium-based battery technology is slowly coming closer to a widespread commercialization. The last couple of decades have been an exciting time for research in the field of Li-ion battery electrode materials. As new materials and strategies are found, Li-ion batteries will no doubt have an ever-lasting greater impact on our lives in the years to come.

Additionally, according to literature reports, Ni-rich layered cathode materials have potential in developing the future-generation of cathode materials for Li-ion batteries. However, the actual challenge that should be given attention is enhancing electrical and mechanical properties of cathode materials. Thus, more studies based on coating with transition metal oxides are necessary. This is because most of transition metals contain d electrons that are loosely bound, contributing to the high electrical conductivity and malleability of these elements. Increasing and strengthening the core-shell synergistic interaction and cross networking of metal oxide layer by increasing surface functional moieties or adding cross-linkers will increase the efficiency of the cathode materials. Furthermore, more research and developments are necessary to improve the literature to help in upgrading electrochemical properties and application of lithium ion batteries. The key to fabricating 3D metal oxide-coated cathode materials is to prepare 3D nanoarchitecture electrodes possessing high capacity at fast charge/discharge rates and improved cyclability. Studies related to the growth of better synthetic routes for metal oxides coated cathode materials, with better controlled composition of oxides that may have an outstanding advantage in the enhancement of the society's economy should be continued.

Author Contributions: Conceptualization, T.R.S. and T.E.M.; methodology, K.D.M.; resources, M.J.H.; data curation, D.M.T.; writing—original draft preparation, T.E.M.; writing—review and editing, T.R.S.; visualization, T.K.S.; supervision, K.D.M.; project administration, B.R.; funding acquisition, K.D.M. All authors have read and agreed to the published version of the manuscript.

Funding: This research was funded by the National Research Foundation of South Africa, NRF UID: 118113 (K.D.M.) and 117727 (M.J.H.).

Institutional Review Board Statement: Not applicable.

Informed Consent Statement: Not applicable.

Conflicts of Interest: The authors declare no conflict of interest.

References

1. Zhang, X. Multiscale understanding and architecture design of high energy/power lithium-ion battery electrodes. *Adv. Energy Mater.* **2021**, *11*, 2000808. [[CrossRef](#)]
2. Erickson, L.E. Reducing greenhouse gas emissions and improving air quality: Two global challenges. *Environ. Prog. Sustain. Energy* **2017**, *36*, 982–988. [[CrossRef](#)]
3. Morgan, J. Electric vehicles: The future we made and the problem of unmaking it. *Camb. J. Econ.* **2020**, *44*, 953–977. [[CrossRef](#)]
4. Von Brockdorff, P.; Gerald, T. Carbon emissions of plug-in electric vehicles in Malta: A policy review. *Case Stud. Transp. Policy* **2017**, *5*, 509–517. [[CrossRef](#)]
5. Nitta, N.; Wu, F.; Lee, J.T.; Yushin, G. Li-ion battery materials: Present and future. *Mater. Today* **2015**, *18*, 252–264. [[CrossRef](#)]
6. Julien, C.M.; Mauger, A.; Zaghib, K.; Groult, H. Comparative issues of cathode materials for Li-ion batteries. *Inorganics* **2014**, *2*, 132–154. [[CrossRef](#)]
7. Gerlach, F.; Hussong, J.; Roisman, I.V.; Tropea, C. A journey through layered cathode materials for lithium ion cells-From lithium cobalt oxide to lithium-rich transition metal oxides. *J. Alloys Compd.* **2020**, *869*, 159239. [[CrossRef](#)]
8. Yao, L.; Xi, Y.; Han, H.; Li, W.; Wang, C.; Feng, Y. LiMn₂O₄ prepared from waste lithium ion batteries through sol-gel process. *J. Alloys Compd.* **2021**, *868*, 159222. [[CrossRef](#)]
9. Huang, Y.; Dong, Y.; Li, S.; Lee, J.; Wang, C.; Zhu, Z.; Xue, W.; Li, Y.; Li, J. Lithium manganese spinel cathodes for lithium-ion batteries. *Adv. Energy Mater.* **2021**, *11*, 2000997. [[CrossRef](#)]

10. Alsamet, M.A.; Burgaz, E. Synthesis and characterization of nano-sized LiFePO_4 by using consecutive combination of sol-gel and hydrothermal methods. *Electrochim. Acta* **2021**, *367*, 137530. [[CrossRef](#)]
11. Shi, Y. Tortuosity modulation toward high-energy and high-power lithium metal batteries. *Adv. Energy Mater.* **2021**, *11*, 2003663. [[CrossRef](#)]
12. Das, T.; Tosoni, S.; Pacchioni, G. Layered oxides as cathode materials for beyond-Li batteries: A computational study of Ca and Al intercalation in bulk V_2O_5 and MoO_3 . *Comput. Mater. Sci.* **2021**, *191*, 110324. [[CrossRef](#)]
13. Sahana, M.B.; Raghavan, G. Recent developments in electrode materials for lithium-ion batteries for energy storage application. In *Handbook of Advanced Ceramics and Composites: Defense, Security, Aerospace and Energy Applications*; Springer: Cham, Switzerland, 2021; pp. 1297–1333.
14. Wu, Y.; Huang, X.; Huang, L.; Chen, J. Strategies for rational design of high-power lithium-ion batteries. *Energy Environ. Mater.* **2021**, *4*, 19–45. [[CrossRef](#)]
15. Zhu, L.; Bao, C.; Xie, L.; Yang, X.; Cao, X. Review of synthesis and structural optimization of $\text{LiNi}_{1/3}\text{Co}_{1/3}\text{Mn}_{1/3}\text{O}_2$ cathode materials for lithium-ion batteries applications. *J. Alloys Compd.* **2020**, *831*, 154864. [[CrossRef](#)]
16. Pender, J.P.; Jha, G.; Youn, D.H.; Ziegler, J.M.; Andoni, I.; Choi, E.J.; Heller, A. Electrode degradation in lithium-ion batteries. *ACS Nano* **2020**, *14*, 1243–1295. [[CrossRef](#)]
17. Han, X.; Lu, L.; Zheng, Y.; Feng, X.; Li, Z.; Li, J.; Ouyang, M. A review on the key issues of the lithium-ion battery degradation among the whole life cycle. *ETransportation* **2019**, *1*, 100005. [[CrossRef](#)]
18. Hausbrand, S.R.; Cherkashinin, G.; Ehrenberg, H.; Grötting, G.; Albe, K.; Hess, C.; Jaegermann, W. Fundamental degradation mechanisms of layered oxide Li-ion battery cathode materials: Methodology, insights and novel approaches. *Mater. Sci. Technol. B* **2015**, *192*, 3–25.
19. Shaw, L.; Ashuri, M. Coating—A potent method to enhance electrochemical performance of $\text{Li}(\text{Ni}_x\text{MnyCo}_z)\text{O}_2$ cathodes for Li-ion batteries. *Adv. Mater. Lett.* **2019**, *10*, 369–380. [[CrossRef](#)]
20. Guan, P.; Zhou, L.; Yu, Z.; Sun, Y.; Liu, Y.; Wu, F.; Jiang, Y.; Chu, D. Recent progress of surface coating on cathode materials for high-performance lithium-ion batteries. *J. Energy Chem.* **2020**, *43*, 220–235. [[CrossRef](#)]
21. Chen, Z.; Qin, Y.; Amine, K.; Sun, Y.K. Role of surface coating on cathode materials for lithium-ion batteries. *J. Mater. Chem.* **2010**, *20*, 7606–7612. [[CrossRef](#)]
22. Somo, T.R.; Mabokela, T.E.; Teffu, D.M.; Sekgobela, T.K.; Hato, M.J.; Modibane, K.D. Review on the effect of metal oxides as surface coatings on hydrogen storage properties of porous and non-porous materials. *Chem. Pap.* **2021**, *10*, 1. [[CrossRef](#)]
23. Oh, Y.; Nam, S.; Wi, S.; Hong, S.; Park, B. Nanoscale interface control for high-performance Li-ion batteries. *Electron. Mater. Lett.* **2012**, *8*, 91–105. [[CrossRef](#)]
24. Wu, J.; Yang, S.; Cai, W.; Bi, Z.; Shang, G.; Yao, J. Multi-characterization of LiCoO_2 cathode films using advanced AFM-based techniques with high resolution. *Sci. Rep.* **2017**, *7*, 11164. [[CrossRef](#)]
25. Swallow, J.G.; Woodford, W.H.; McGrogan, F.P.; Ferralis, N.; Chiang, Y.-M.; Van Vliet, K.J. Effect of electrochemical charging on elastoplastic properties and fracture toughness of Li_xCoO_2 . *J. Electrochem. Soc.* **2014**, *161*, F3084–F3090. [[CrossRef](#)]
26. Demirocak, D.E.; Bhushan, B. Probing the aging effects on nanomechanical properties of a LiFePO_4 cathode in a large format prismatic cell. *J. Power Sources* **2015**, *280*, 256–262. [[CrossRef](#)]
27. Hao, X.; Lin, X.; Lu, W.; Bartlett, B.M. Oxygen vacancies lead to loss of domain order, particle fracture, and rapid capacity fade in lithium manganospinel (LiMn_2O_4) batteries. *ACS Appl. Mater. Interfaces* **2014**, *6*, 10849–10857. [[CrossRef](#)] [[PubMed](#)]
28. Cheng, H.M.; Wang, F.M.; Chu, J.P.; Santhanam, R.; Rick, J.; Lo, S.C. Enhanced cycleability in lithium ion batteries: Resulting from atomic layer deposition of Al_2O_3 or TiO_2 on LiCoO_2 electrodes. *J. Phys. Chem. C* **2012**, *116*, 7629–7637. [[CrossRef](#)]
29. Zhou, A.; Dai, X.; Lu, Y.; Wang, Q.; Fu, M.; Li, J. Enhanced interfacial kinetics and high-voltage/high-rate performance of LiCoO_2 cathode by controlled sputter-coating with a nanoscale $\text{Li}_4\text{Ti}_5\text{O}_{12}$ ionic conductor. *ACS Appl. Mater. Interfaces* **2016**, *8*, 34123–34131. [[CrossRef](#)] [[PubMed](#)]
30. Nazri, G.A.; Pistoia, G. *Lithium Batteries: Science and Technology*; Springer Science and Business Media: Berlin/Heidelberg, Germany, 2008; pp. 112–153.
31. Wang, C.W. High-voltage LiCoO_2 material encapsulated in a $\text{Li}_4\text{Ti}_5\text{O}_{12}$ ultrathin layer by high-speed solid-phase coating process. *ACS Appl. Energy Mater.* **2020**, *3*, 2593–2603. [[CrossRef](#)]
32. Cho, J.; Kim, Y.J.; Kim, T.J.; Park, B. Zero-strain intercalation cathode for rechargeable Li-Ion cell. *Angew. Chem. Int. Ed.* **2001**, *40*, 3367–3369. [[CrossRef](#)]
33. Bratosin, I.; Ghica, V.G.; Petrescu, M.I.; Buzatu, M.; Iacob, G.; Necşulescu, A.D. Researches on the recovery of useful metals from spent Li-Ion batteries. *IOP Conf. Ser. Mater. Sci. Eng.* **2021**, *1037*, 012039. [[CrossRef](#)]
34. Jiang, H.; Chen, X.; Liu, Y.; Zhao, Q.; Li, H.; Chen, B. Online state-of-charge estimation based on the gas–liquid dynamics model for $\text{Li}(\text{NiMnCo})\text{O}_2$ battery. *Energies* **2021**, *14*, 324. [[CrossRef](#)]
35. Wang, Y. Pillar-beam structures prevent layered cathode materials from destructive phase transitions. *Nat. Commun.* **2021**, *12*, 13. [[CrossRef](#)]
36. Zhang, C.; Jiang, W.; He, W.; Wei, W. Heteroepitaxial interface of layered cathode materials for lithium ion batteries. *Energy Storage Mater.* **2021**, *37*, 161–189. [[CrossRef](#)]
37. Chen, X.; Song, J.; Li, J.; Zhang, H.; Tang, H. A P2/P3 composite-layered cathode material with low-voltage decay for sodium-ion batteries. *J. Appl. Electrochem.* **2021**. [[CrossRef](#)]

38. Seo, J.Y.; Oh, D.; Kim, D.J.; Kim, K.M.; Kwon, J.S. Enhanced mechanical properties of ZrO₂-Al₂O₃ dental ceramic composites by altering Al₂O₃ form. *Dent. Mater.* **2020**, *36*, 117–125. [[CrossRef](#)] [[PubMed](#)]
39. Chung, K.Y. In situ XRD studies of the structural changes of ZrO₂-coated LiCoO₂ during cycling and their effects on capacity retention in lithium batteries. *J. Power Sources* **2006**, *163*, 185–190. [[CrossRef](#)]
40. Liu, L. Electrochemical and in situ synchrotron XRD studies on Al₂O₃-coated LiCoO₂ cathode material. *J. Electrochem. Soc.* **2004**, *151*, A1344. [[CrossRef](#)]
41. Jaephil, C.; Chan-Soo, K.; Sang-Im, Y. Improvement of structural stability of LiCoO₂ cathode during electrochemical cycling by sol-gel coating of SnO₂. *Electrochem. Solid-State Lett.* **2000**, *3*, 362–365. [[CrossRef](#)]
42. Fey, G.T.K.; Muralidharan, P.; Lu, C.Z.; Da Cho, Y. Enhanced electrochemical performance and thermal stability of La₂O₃-coated LiCoO₂. *Electrochim. Acta* **2006**, *51*, 4850–4858. [[CrossRef](#)]
43. Kim, K.; Ha, H.W.; Yun, N.J.; Kim, M.H.; Woo, M.H. Enhanced electrochemical and thermal stability of surface-modified LiCoO₂ cathode by CeO₂ coating. *Electrochim. Acta* **2006**, *51*, 3297–3302. [[CrossRef](#)]
44. Xi, Z.; Wang, Z.; Peng, W.; Guo, H.L.; Wang, J. Effect of copper and iron substitution on the structures and electrochemical properties of LiNi_{0.8}Co_{0.15}Al_{0.05}O₂ cathode materials. *Energy Sci. Eng.* **2020**, *8*, 1868–1879. [[CrossRef](#)]
45. Kim, Y.J.; Cho, J.; Kim, T.J.; Park, B. Suppression of cobalt dissolution from the LiCoO₂ cathodes with various metal-oxide coatings. *J. Electrochem. Soc.* **2003**, *150*, A1723. [[CrossRef](#)]
46. Wu, H.; Jia, H.; Wang, C.; Zhang, J.G.; Xu, W. Recent progress in understanding solid electrolyte interphase on lithium metal anodes. *Adv. Energy Mater.* **2021**, *11*, 2003092. [[CrossRef](#)]
47. Myung, S.T.; Izumi, K.; Komaba, S.; Sun, Y.K.; Yashiro, H.; Kumagai, N. Role of alumina coating on Li-Ni-Co-Mn-O particles as positive electrode material for lithium-ion batteries. *Chem. Mater.* **2005**, *17*, 3695–3704. [[CrossRef](#)]
48. Aykol, M.; Kirklin, S.; Wolverton, C. Thermodynamic aspects of cathode coatings for lithium-ion batteries. *Adv. Energy Mater.* **2014**, *4*, 1400690. [[CrossRef](#)]
49. Shim, J.H.; Lee, S.; Park, S.S. Effects of MgO coating on the structural and electrochemical characteristics of LiCoO₂ as cathode materials for lithium ion battery. *Chem. Mater.* **2014**, *26*, 2537–2543. [[CrossRef](#)]
50. Sayle, T.X.T.; Caddeo, F.; Monama, N.O.; Kgwane, K.M.; Ngoepe, P.E.; Sayle, D.C. Origin of electrochemical activity in nano-Li₂MnO₃; Stabilization via a ‘point defect scaffold’. *Nanoscale* **2015**, *7*, 1167–1180. [[CrossRef](#)]
51. He, S. Al-Ti-oxide coated LiCoO₂ cathode material with enhanced electrochemical performance at a high cutoff charge potential of 4.5 V. *J. Alloys Compd.* **2019**, *799*, 137–146. [[CrossRef](#)]
52. Lee, J.W.; Park, S.M.; Kim, H.J. Enhanced cycleability of LiCoO₂ coated with vanadium oxides. *J. Power Sources* **2009**, *188*, 583–587. [[CrossRef](#)]
53. Hao, Q. Nano-CuO coated LiCoO₂: Synthesis, improved cycling stability and good performance at high rates. *Electrochim. Acta* **2011**, *56*, 9027–9031. [[CrossRef](#)]
54. Dai, X.; Wang, L.; Xu, J.; Wang, Y.; Zhou, A.; Li, J. Improved electrochemical performance of LiCoO₂ electrodes with ZnO coating by radio frequency magnetron sputtering. *ACS Appl. Mater. Interfaces* **2014**, *6*, 15853–15859. [[CrossRef](#)]
55. Liu, G.Q. Study of electrochemical properties of coating ZrO₂ on LiCoO₂. *J. Alloys Compd.* **2010**, *496*, 512–516. [[CrossRef](#)]
56. Jayasree, S.S.; Nair, S.; Santhanagopalan, D. Ultrathin TiO₂ coating on LiCoO₂ for improved electrochemical performance as Li-ion battery cathode. *ChemistrySelect* **2018**, *3*, 2763–2766. [[CrossRef](#)]
57. Zhang, Z.; Gong, Z.; Yang, Y. Electrochemical performance and surface properties of bare and TiO₂-coated cathode materials in lithium-ion batteries. *J. Phys. Chem. B* **2004**, *108*, 17546–17552. [[CrossRef](#)]
58. Zhang, C.; Liu, X.; Su, Q.; Wu, J.; Huang, T.; Yu, A. Enhancing electrochemical performance of LiMn₂O₄ cathode material at elevated temperature by uniform nanosized TiO₂ coating. *ACS Sustain. Chem. Eng.* **2017**, *5*, 640–647. [[CrossRef](#)]
59. Waller, G.H. Structure and surface chemistry of Al₂O₃ coated LiMn₂O₄ nanostructured electrodes with improved lifetime. *J. Power Sources* **2016**, *306*, 162–170. [[CrossRef](#)]
60. Tao, S. Enhanced electrochemical performance of MoO₃-coated LiMn₂O₄ cathode for rechargeable lithium-ion batteries. *Mater. Chem. Phys.* **2017**, *199*, 203–208. [[CrossRef](#)]
61. Xia, H.; Luo, Z.; Xie, J. Nanostructured LiMn₂O₄ and their composites as high-performance cathodes for lithium-ion batteries. *Prog. Nat. Sci. Mater. Int.* **2012**, *22*, 572–584. [[CrossRef](#)]
62. Thackeray, M.M. Exploiting the spinel structure for Li-ion battery applications: A tribute to John B. Goodenough. *Adv. Energy Mater.* **2021**, *11*, 2001117. [[CrossRef](#)]
63. Liu, D.; Su, W.; Wang, L. Pyrometallurgically regenerated LiMn₂O₄ cathode scrap material and its electrochemical properties. *Ceram. Int.* **2021**, *47*, 42–47. [[CrossRef](#)]
64. Tesfamhret, Y.; Liu, H.; Chai, Z.; Berg, E.; Younesi, R. On the manganese dissolution process from LiMn₂O₄ cathode material. *ChemElectroChem* **2021**. [[CrossRef](#)]
65. Rodríguez, A.R. Unveiling the role of Mn-interstitial defect and particle size on the Jahn-Teller distortion of the LiMn₂O₄ cathode material. *J. Power Sources* **2021**, *490*, 229519. [[CrossRef](#)]
66. Choi, N.S.; Han, J.G.; Ha, S.Y.; Park, I.; Back, C.K. Recent advances in the electrolytes for interfacial stability of high-voltage cathodes in lithium-ion batteries. *RSC Adv.* **2015**, *5*, 2732–2748. [[CrossRef](#)]
67. Deepi, A.S.; Srikesh, G.; Nesaraj, A.S. Combustion synthesis and characterization of Ni-doped LiMn₂O₄ cathode nanoparticles for lithium ion battery applications. *Rev. Mater.* **2021**, *26*. [[CrossRef](#)]

68. Chen, L.; Warburton, R.E.; Chen, K.S.; Libera, J.A.; Johnson, C.; Yang, Z.; Hersam, M.C.; Greeley, J.P.; Elam, J.W. Mechanism for Al_2O_3 atomic layer deposition on LiMn_2O_4 from in situ measurements and ab initio calculations. *Chem* **2018**, *4*, 2418–2435. [[CrossRef](#)]
69. Warburton, R.E.; Young, M.J.; Letourneau, S.; Elam, J.W.; Greeley, J. Descriptor-based analysis of atomic layer deposition mechanisms on spinel LiMn_2O_4 lithium-ion battery cathodes. *Chem. Mater.* **2020**, *32*, 1794–1806. [[CrossRef](#)]
70. Ouyang, C.Y.; Zeng, X.M.; Slijvancanin, Z.; Baldereschi, A. Oxidation states of Mn atoms at clean and Al_2O_3 -covered LiMn_2O_4 (001) surfaces. *J. Phys. Chem. C* **2010**, *114*, 4756–4759. [[CrossRef](#)]
71. Feng, X.; Zhang, J.; Yin, L. Enhanced cyclic stability of spinel LiMn_2O_4 for lithium-ion batteries by surface coating with WO_3 . *Energy Technol.* **2016**, *4*, 490–495. [[CrossRef](#)]
72. Ming, H. Gradient V_2O_5 surface-coated LiMn_2O_4 cathode towards enhanced performance in Li-ion battery applications. *Electrochim. Acta* **2014**, *120*, 390–397. [[CrossRef](#)]
73. Zhu, H.; Miao, C.; Guo, R.; Liu, Y.; Wang, X. A simple and low-cost synthesis strategy of LiFePO_4 nanoparticles as cathode materials for lithium ion batteries. *Int. J. Electrochem. Sci.* **2021**, *16*, 210331. [[CrossRef](#)]
74. Shi, M.; Li, R.; Liu, Y. In situ preparation of LiFePO_4/C with unique copolymer carbon resource for superior performance lithium-ion batteries. *J. Alloys Compd.* **2021**, *854*, 157162. [[CrossRef](#)]
75. Luo, G.Y. Electrochemical performance of in situ LiFePO_4 modified by N-doped graphene for Li-ion batteries. *Ceram. Int.* **2020**, *12*, 259. [[CrossRef](#)]
76. Omid, A.H.; Babaei, A.; Ataie, A. Low temperature synthesis of nanostructured LiFePO_4/C cathode material for lithium ion batteries. *Mater. Res. Bull.* **2020**, *125*, 110807. [[CrossRef](#)]
77. Sumanov, V.D.; Tyablikov, O.A.; Morozov, A.V.; Fedotov, S.S.; Vassiliev, S.Y.; Nikitina, V.A. Phase boundary propagation mode in nano-sized electrode materials evidenced by potentiostatic current transients analysis: Li-rich LiFePO_4 case study. *Electrochim. Acta* **2021**, *368*, 137627. [[CrossRef](#)]
78. Lee, S.J.; Nam, Y.C.; Son, J.T. Comparison between conventional nano-sized and honeycomb-shaped LiFePO_4 cathode materials for Li-ion batteries. *J. Korean Phys. Soc.* **2020**, *77*, 505–509. [[CrossRef](#)]
79. Tian, X.; Chen, W.; Jiang, Z.; Jiang, Z.J. Porous carbon-coated LiFePO_4 nanocrystals prepared by in situ plasma-assisted pyrolysis as superior cathode materials for lithium ion batteries. *Ionics* **2020**, *26*, 2715–2726. [[CrossRef](#)]
80. Wang, X. Fluorine doped carbon coating of LiFePO_4 as a cathode material for lithium-ion batteries. *Chem. Eng. J.* **2020**, *379*, 122371. [[CrossRef](#)]
81. Zhang, J. Binary carbon-based additives in LiFePO_4 cathode with favorable lithium storage. *Nanotechnol. Rev.* **2020**, *9*, 934–944. [[CrossRef](#)]
82. Subba Reddy, C.V.; Chen, M.; Jin, W.; Zhu, Q.Y.; Chen, W.; Mho, S. Characterization of (PVDF + LiFePO_4) solid polymer electrolyte. *J. Appl. Electrochem.* **2007**, *37*, 637–642. [[CrossRef](#)]
83. Sun, Q. Resynthesizing LiFePO_4/C materials from the recycled cathode via a green full-solid route. *J. Alloys Compd.* **2020**, *818*, 153292. [[CrossRef](#)]
84. Dhaybi, S.; Marsan, B.; Hammami, A. A novel low-cost and simple colloidal route for preparing high-performance carbon-coated LiFePO_4 for lithium batteries. *J. Energy Storage* **2018**, *18*, 259–265. [[CrossRef](#)]
85. Tang, H.; Tan, L.; Xu, J. Synthesis and characterization of LiFePO_4 coating with aluminum doped zinc oxide. *Trans. Nonferrous Met. Soc. China Engl. Ed.* **2013**, *23*, 451–455. [[CrossRef](#)]
86. Liu, H.; Wang, G.X.; Wexler, D.; Wang, J.Z.; Liu, H.K. Electrochemical performance of LiFePO_4 cathode material coated with ZrO_2 nanolayer. *Electrochem. Commun.* **2008**, *10*, 165–169. [[CrossRef](#)]
87. Chang, H.H.; Chang, C.C.; Su, C.Y.; Wu, H.C.; Yang, M.H.; Wu, N.L. Effects of TiO_2 coating on high-temperature cycle performance of LiFePO_4 -based lithium-ion batteries. *J. Power Sources* **2008**, *185*, 466–472. [[CrossRef](#)]
88. Cui, Y.; Zhao, X.; Guo, R. Enhanced electrochemical properties of LiFePO_4 cathode material by CuO and carbon co-coating. *J. Alloys Compd.* **2010**, *490*, 236–240. [[CrossRef](#)]
89. Cui, Y.; Zhao, X.; Guo, R. High rate electrochemical performances of nanosized ZnO and carbon co-coated LiFePO_4 cathode. *Mater. Res. Bull.* **2010**, *45*, 844–849. [[CrossRef](#)]
90. Jin, Y.; Yang, C.P.; Rui, C.H.; Cheng, T.; Chen, C.H. V_2O_3 modified LiFePO_4/C composite with improved electrochemical performance. *J. Power Sources* **2011**, *196*, 5623–5630. [[CrossRef](#)]
91. Bosch-Jimenez, P. Non-precious metal doped carbon nanofiber air-cathode for Microbial Fuel Cells application: Oxygen reduction reaction characterization and long-term validation. *Electrochim. Acta* **2017**, *228*, 380–388. [[CrossRef](#)]
92. Hu, G.-R.; Deng, X.-R.; Peng, Z.-D.; Du, K. Comparison of AlPO_4 - and $\text{Co}_3(\text{PO}_4)_2$ -coated $\text{LiNi}_{0.8}\text{Co}_{0.2}\text{O}_2$ cathode materials for Li-ion battery. *Electrochim. Acta* **2008**, *53*, 2567–2573.
93. Zhang, Y.; Huo, Q.Y.; Du, P.P.; Wang, L.Z.; Zhang, A.Q.; Song, Y.H.; Li, G.Y. Advances in new cathode material LiFePO_4 for lithium-ion batteries. *Synth. Met.* **2012**, *162*, 1315–1326. [[CrossRef](#)]
94. Li, Y.D.; Zhao, S.X.; Nan, C.W.; Li, B.H. Electrochemical performance of SiO_2 -coated LiFePO_4 cathode materials for lithium ion battery. *J. Alloys Compd.* **2011**, *509*, 957–960. [[CrossRef](#)]
95. Yao, J.; Wu, F.; Qiu, X.; Li, N.; Su, Y. Effect of CeO_2 -coating on the electrochemical performances of LiFePO_4/C cathode material. *Electrochim. Acta* **2011**, *56*, 5587–5592. [[CrossRef](#)]